

# IEEE 802.15.4a channel model - final report

Andreas F. Molisch, Kannan Balakrishnan, Dajana Cassioli, Chia-Chin Chong, Shahriar Emami, Andrew Fort, Johan Karedal, Juergen Kunisch, Hans Schantz, Ulrich Schuster, Kai Siwiak

## Abstract

This is a discussion document for the IEEE document of the IEEE 802.15.4a channel modeling subgroup. It provides models for the following frequency ranges and environments: for UWB channels covering the frequency range from 2 to 10 GHz, it covers indoor residential, indoor office, industrial, outdoor, and open outdoor environments (usually with a distinction between LOS and NLOS properties). For the frequency range from 2 to 6 GHz, it gives a model for body area networks. For the frequency range from 100 to 900 MHz, it gives a model for indoor office-type environments. Finally, for a 1MHz carrier frequency, a narrowband model is given. The document also provides MATLAB programs and numerical values for 100 impulse response realizations in each environment.

## I. INTRODUCTION

### A. Background and goals of the model

This document summarizes the activities and recommendations of the channel modeling subgroup of IEEE 802.15.4a. The Task Group 802.15.4a has the mandate to develop an alternative physical layer for sensor networks and similar devices, working with the IEEE 802.15.4 MAC layer. The main goals for this new standard are energy-efficient data communications with data rates between 1kbit/s and several Mbit/s; additionally, the capability for geolocation plays an important role. More details about the goals of the task group can be found in the IEEE 802.15.4a PAR. In order to evaluate different forthcoming proposals, channel models are required. The main goal of those channel models is a fair comparison of different proposals. They are not intended to provide information of absolute performance in different environments. Though great efforts have been made to make the models as realistic as possible, the number of available measurements on which the model can be based, both in the 3 – 10 GHz range, and in the 100-1000 MHz range, is insufficient for that purpose; furthermore, it was acceptable to do some (over)simplifications that affect the absolute performance, but not the relative behavior of the different proposals.

A major challenge for the channel modeling activities derived from the fact that the PAR and call for proposals does not mandate a specific technology, and not even a specific frequency range. For this reason, this document contains three different models:

- an ultrawideband (UWB) model, spanning the frequency range from 2 to 10 GHz. Models for any narrowband system within that frequency range can be derived by a simple bandpass filtering operation.
- an ultrawideband model for the frequency range from 100-1000 MHz. Again, narrowband systems located within that frequency range can obtain their specific model by filtering.
- a narrowband model for the frequency range around 1 MHz.

The generic structure of the UWB models for the two considered frequency ranges is rather similar, but the parameterizations are different. The model structure for the 1MHz model is fundamentally different. All the models are time-continuous; the temporal discretization (which is required for any simulation) is left to the implementer. To further facilitate the use of the model, this document also includes a MATLAB program for the generation of impulse responses, as well as Excel tables of impulse responses. The use of these stored impulse responses are mandatory for the simulations of systems submitted to 802.15.4a

The main goals of the model were the modeling of attenuation and delay dispersion. The former subsumes both shadowing and average pathloss, while the latter describes the power delay profile and the small-scale fading statistics; from this, other parameters such as rms delay spread, number of multipath components carrying  $x\%$  of the energy, etc. However, for the simulations within 15.4a, it was decided to *not* include shadowing.

The channel modeling subgroup started its activities at the meeting in September 2003 (Singapore), and is submitting this final report in November 2004 (San Antonio) for vote by the full group; minor modifications and eliminations of typos are presented in this latest version, submitted for the meeting in January 2005 (Monterey). During the course of this year, progress was made mainly through bi-weekly phone conferences as well as at the IEEE 802 meetings (see also [04-024] [04-195] [04-346] [04-204] [04-345]). A large number of documents on specific topics has been presented to the subgroup at the IEEE 802 meetings; they can be found on the [www.802wirelessworld.com](http://www.802wirelessworld.com) server, and are cited where appropriate in this document. Appreciation is extended to all the participants from academia and industry, whose efforts made this model possible./

The remainder of the document is organized the following way: Section II gives an overview of the considered environments, as well as the definitions of the channel parameters that will be used in later sections. Section III describes and IV contain the parameterizations for the 2 – 10 GHz and the 100 – 1000MHz range, respectively. Section V describes the structure and parameterization of the model for body-area networks, which is different from the other environments. Next, we describe the narrowband model for 1MHz. A summary and conclusion wrap up the report. Appendix A contain a summary of all measurement documents and proposals presented to the group; a MATLAB program for the generation of impulse responses, can be found

in Appendix B, and general procedures for the measurement and the evaluation of the data, as recommended by the modeling subgroup are contained in Appendix C.

## B. Environments

From the "call for applications", we derived a number of environments in which 802.15.4a devices should be operating. This list is not comprehensive, and cannot cover all possible future applications; however, it should be sufficient for the evaluation of the model:

- 1) Indoor residential: these environments are critical for "home networking", linking different appliances, as well as danger (fire, smoke) sensors over a relatively small area. The building structures of residential environments are characterized by small units, with indoor walls of reasonable thickness.
- 2) Indoor office: for office environments, some of the rooms are comparable in size to residential, but other rooms (especially cubicle areas, laboratories, etc.) are considerably larger. Areas with many small offices are typically linked by long corridors. Each of the offices typically contains furniture, bookshelves on the walls, etc., which adds to the attenuation given by the (typically thin) office partitionings.
- 3) Industrial environments: are characterized by larger enclosures (factory halls), filled with a large number of metallic reflectors. This is anticipated to lead to severe multipath.
- 4) Body-area network (BAN): communication between devices located on the body, e.g., for medical sensor communications, "wearable" cellphones, etc. Due to the fact that the main scatterers is in the nearfield of the antenna, and the generally short distances, the channel model can be anticipated to be quite different from the other environments.
- 5) Outdoor. While a large number of different outdoor scenarios exist, the current model covers only a suburban-like microcell scenario, with a rather small range.
- 6) Agricultural areas/farms: for those areas, few propagation obstacles (silos, animal pens), with large distances in between, are present. Delay spread can thus be anticipated to be smaller than in other environments

*Remark 1:* another important environments are disaster areas, like propagation through avalanches in the model, for the recovery of victims. Related important applications would include propagation through rubble (e.g., after an earthquake), again for victim recovery and communications between emergency personnel. Unfortunately, no measurement data are available for these cases.

## II. GENERIC CHANNEL MODEL

In this chapter, we describe the generic channel model that is used for both the 100-1000MHz and the 2-10 GHz model. An exception to this case is the "body-area network", which shows a different generic structure, and thus will be treated in a separate chapter. Also, the structure for the 1MHz model is different, and will be treated in a separate chapter.

Before going into details, we summarize the key features of the model:

- model treats only channel, while antenna effects are to be modeled separately
- $d^{-n}$  law for the pathloss
- frequency dependence of the pathloss
- modified Saleh-Valenzuela model:
  - arrival of paths in clusters
  - mixed Poisson distribution for ray arrival times
  - possible delay dependence of cluster decay times
  - some NLOS environments have first increase, then decrease of power delay profile
- Nakagami-distribution of small-scale fading, with different  $m$ -factors for different components
- block fading: channel stays constant over data burst duration

### A. Pathloss - preliminary comments

The path gain in a narrowband system is conventionally defined as

$$G(d) = \frac{E\{P_{RX}(d, f_c)\}}{P_{TX}} \quad (1)$$

where  $P_{TX}$  and  $P_{RX}$  are transmit and receive power, respectively, as seen at the antenna connectors of transmitter and receiver,  $d$  is the distance between transmitter and receiver,  $f_c$  is the center frequency, and the expectation  $E\{\cdot\}$  is taken over an area that is large enough to allow averaging out of the shadowing as well as the small-scale fading  $E\{\cdot\} = E_{lsf}\{E_{ssf}\{\cdot\}\}$ , where "lsf" and "ssf" indicate large-scale fading and small-scale fading, respectively. Note that we use the common name "pathloss", though "path gain" would be a better description (PL as defined above). Due to the frequency dependence of propagation effects

in a UWB channel, the wideband pathloss is a function of frequency as well as of distance. It thus makes sense to define a *frequency-dependent pathloss* (related to wideband pathloss suggested in Refs. [1], [2])

$$G(f, d) = \frac{1}{\Delta} E \left\{ \int_{f-\Delta f/2}^{f+\Delta f/2} |H(\tilde{f}, d)|^2 d\tilde{f} \right\} \quad (2)$$

where  $H(f, d)$  is the transfer function from antenna connector to antenna connector, and  $\Delta f$  is chosen small enough so that diffraction coefficients, dielectric constants, etc., can be considered constant within that bandwidth; the *total* pathloss is obtained by integrating over the whole bandwidth of interest.<sup>1</sup> Integration over the frequency and expectation  $E_{ssf}\{\}$  thus essentially have the same effect, namely averaging out the small-scale fading.

To simplify computations, we assume that the pathloss as a function of the distance and frequency can be written as a product of the terms

$$G(f, d) = \overline{G}(f) \tilde{G}(d). \quad (3)$$

The frequency dependence of the pathloss is given as [3], [4]

$$\sqrt{\tilde{G}(f)} \propto f^{-\kappa} \quad (4)$$

*Remark 2:* Note that the system proposer has to provide (and justify) data for the frequency dependence of the antenna characteristics. Antennas are *not* included in the channel model !!! (see also next subsection).

The distance dependence of the pathloss in dB is described by

$$\overline{G}(d) = G_0 - 10n \log_{10} \left( \frac{d}{d_0} \right) \quad (5)$$

where the reference distance  $d_0$  is set to 1 m, and  $G_0$  is the pathloss at the reference distance.  $n$  is the pathloss exponent. The pathloss exponent also depends on the environment, and on whether a line-of-sight (LOS) connection exists between the transmitter and receiver or not. Some papers even further differentiate between LOS, "soft" NLOS (non-LOS), also known as "obstructed LOS" (OLOS), and "hard NLOS". LOS pathloss exponents in indoor environments range from 1.0 in a corridor [5] to about 2 in an office environment. NLOS exponents typically range from 3 to 4 for soft NLOS, and 4 – 7 for hard NLOS. Note that this model is no different from the most common narrowband channel models. The many results available in the literature for this case can thus be re-used.

*Remark 3:* the above model for the distance dependence of the pathloss is known as "power law". Another model, which has been widely used, is the "breakpoint model", where different attenuation exponents are valid in different distance ranges. Due to the limited availability of measurement data, and concerns for keeping the simulation procedure simple, we decided not to use this breakpoint model for our purposes.

*Remark 4:* Refs. [6], [7], [8], [9], had suggested to model the pathloss exponent as a random variable that changes from building to building, specifically as a Gaussian distribution. The distribution of the pathloss exponents will be truncated to make sure that only physically reasonable exponents are chosen. This approach shows good agreement with measured data; however, it leads to a significant complication of the simulation procedure prescribed within 802.15.4a, and thus was not adopted for our model.

## B. Pathloss - recommended model

The above model includes the effects of the transmit and the receive antenna, as it defines the pathloss as the ratio of the received power at the RX antenna connector, divided by the transmit power (as seen at the TX antenna connector). However, we can anticipate that different proposals will have quite different antennas, depending on their frequency range, and also depending on their specific applications. We therefore present in this section a model that model describes the channel only, while excluding antenna effects. The system proposers are to present an antenna model as part of their proposal, specifying the key antenna parameters (like antenna efficiency, form factor, etc.). Especially, we find that the proposer has to specify the frequency dependence of the antenna efficiency. Furthermore, we note that the model is not direction-dependent. consequently, it is not possible to include the antenna gain in the computations.

The computation of the received power should proceed the following way:

- 1) in a first step, the proposer has to define the transmit power spectrum that will be seen "on air". This spectrum is the product of the output spectrum of the transmit amplifier, i.e., as seen at the antenna connector (it will in many cases approximate the FCC mask quite well) with the frequency dependent antenna efficiency.<sup>2</sup>

$$P_{\text{TX}}(f) = P_{\text{TX-amp}}(f) \cdot \eta_{\text{TX-ant}}(f) \quad (6)$$

<sup>1</sup>Note that the transfer function in the frequency selective case is  $H(f) = P_{RX}(f)/P_{TX}(f)$ , where  $P_{RX}(f)$  and  $P_{TX}(f)$  are now power spectral densities.

<sup>2</sup>Note that the frequency dependence of the antenna gain does not play a role here, as it only determines the distribution of the energy over the spatial angles - but our computations average over the spatial angle.

The proposer has to make sure that this "on air" spectrum fulfills the regulations of the relevant national frequency regulators, especially the requirements of the FCC. Note that the FCC has specified a power spectral density at a distance of 1m from the transmit antenna. It is anticipated that due to the typical falloff of antenna efficiency with frequency, the "on-air" power is lower for high frequencies.

- 2) In a next step, we compute the frequency-dependent power density at a distance  $d$ , as

$$\widehat{P}(f, d) = K_0 \frac{P_{\text{TX}}(f)}{4\pi d_0^2} \left(\frac{d}{d_0}\right)^{-n} \left(\frac{f}{f_c}\right)^{-2\kappa} \quad (7)$$

where the normalization constant  $K_0$  will be determined later on. Note that this reverts to the conventional picture of energy spreading out equally over the surface of a sphere when we set  $n = 2$ , and  $\kappa = 0$ .

- 3) Finally, the received frequency-dependent power has to be determined, by multiplying the power density at the location of the receiver with the antenna area  $A_{\text{RX}}$

$$A_{\text{RX}}(f) = \frac{\lambda^2}{4\pi} G_{\text{RX}}(f) \quad (8)$$

where  $G_{\text{RX}}$  is the receive antenna gain; and also multiply with the antenna efficiency  $\eta_{\text{RX-ant}}(f)$ . Since we are again assuming that the radiation is averaged over all incident angles, the antenna gain (averaged over the different directions) is unity, independent of the considered frequency. The frequency-dependent received power is then given by

$$P_{\text{r}}(d, f) = K_0 P_{\text{TX-amp}}(f) \cdot \eta_{\text{TX-ant}}(f) \eta_{\text{RX-ant}}(f) \frac{c_0^2}{(4\pi d_0 f_c)^2} \frac{1}{(d/d_0)^n (f/f_c)^{2\kappa+2}} \quad (9)$$

The normalization constant  $K_0$  has to be chosen in such a way that the attenuation at distance  $d_0 = 1$  m (the reference distance for all of our scenarios), and at the reference frequency  $f_c = 5$  GHz is equal to a value  $G_0$  that will be given later in the tables, under the assumption of an ideally efficient, isotropic antenna. Thus,

$$\frac{P_{\text{r}}(d_0, f_c)}{P_{\text{TX-amp}}(f_c)} = G_0 = K_0 \frac{c_0^2}{(4\pi d_0 f_c)^2} \quad (10)$$

so that

$$K_0 = \frac{(4\pi d_0 f_c)^2}{c_0^2} G_0 \quad (11)$$

- 4) Finally, it has been shown that the presence of a person (user) close to the antenna will lead to an attenuation. Measurements have shown this process to be stochastic, with attenuations varying between 1dB and more than 10dB, depending on the user [10]. However, we have decided - for the sake of simplicity - to model this process by a "antenna attenuation factor"  $A_{\text{ant}}$  of 1/2 that is fixed, and has to be included in all computations. We therefore find the frequency-dependent path gain to be given by

$$G(d, f) = \frac{P_{\text{r}}(f)}{P_{\text{TX-amp}}(f)} = \frac{1}{2} G_0 \eta_{\text{TX-ant}}(f) \eta_{\text{RX-ant}}(f) \frac{(f/f_c)^{-2(\kappa+1)}}{(d/d_0)^n} \quad (12)$$

For the system proposers, it is important to provide the quantity

$$\widetilde{H}(f) = \frac{1}{2} G_0 \eta_{\text{TX-ant}}(f) \eta_{\text{RX-ant}}(f) \frac{(f/f_c)^{-2}}{(d/d_0)^n} \quad (13)$$

Remember that the antenna efficiencies and their frequency dependence has to be given by the proposer, preferably based on measured values.

### C. Shadowing

Shadowing, or large-scale fading, is defined as the variation of the local mean around the pathloss. Also this process is fairly similar to the narrowband fading. The pathloss (averaged over the small-scale fading) in dB can be written as

$$\overline{G}(d) = G_0 - 10n \log_{10} \left(\frac{d}{d_0}\right) + S \quad (14)$$

where  $S$  is a Gaussian-distributed random variable with zero mean and standard deviation  $\sigma_S$ .

Note that for the simulation procedure according to the selection criteria document, shadowing shall *not* be taken into account!

*Remark 5:* While the shadowing shows a finite coherence time (distance), this is not considered in the model. The simulation procedure in 802.154a prescribes that each data packet is transmitted in a different channel realization, so that correlations of the shadowing from one packet to the next are not required/allowed in the simulations.

#### D. Power delay profile

The impulse response (in complex baseband) of the SV (Saleh-Valenzuela) model is given in general as [11]

$$h_{discr}(t) = \sum_{l=0}^L \sum_{k=0}^K a_{k,l} \exp(j\phi_{k,l}) \delta(t - T_l - \tau_{k,l}), \quad (15)$$

where  $a_{k,l}$  is the tap weight of the  $k^{th}$  component in the  $l$ th cluster,  $T_l$  is the delay of the  $l$ th cluster,  $\tau_{k,l}$  is the delay of the  $k$ th MPC relative to the  $l$ -th cluster arrival time  $T_l$ . The phases  $\phi_{k,l}$  are uniformly distributed, i.e., for a bandpass system, the phase is taken as a uniformly distributed random variable from the range  $[0, 2\pi]$ . Following [12], the number of clusters  $L$  is an important parameter of the model. It is assumed to be Poisson-distributed

$$pdf_L(L) = \frac{(\bar{L})^L \exp(-\bar{L})}{L!} \quad (16)$$

so that the mean  $\bar{L}$  completely characterizes the distribution.

By definition, we have  $\tau_{0,l} = 0$ . The distributions of the cluster arrival times are given by a Poisson processes

$$p(T_l | T_{l-1}) = \Lambda_l \exp[-\Lambda_l(T_l - T_{l-1})], \quad l > 0 \quad (17)$$

where  $\Lambda_l$  is the cluster arrival rate (assumed to be independent of  $l$ ). The classical SV model also uses a Poisson process for the ray arrival times. Due to the discrepancy in the fitting for the indoor residential, and indoor and outdoor office environments, we propose to model ray arrival times with mixtures of two Poisson processes as follows

$$p(\tau_{k,l} | \tau_{(k-1),l}) = \beta \lambda_1 \exp[-\lambda_1(\tau_{k,l} - \tau_{(k-1),l})] + (\beta - 1) \lambda_2 \exp[-\lambda_2(\tau_{k,l} - \tau_{(k-1),l})], \quad k > 0 \quad (18)$$

where  $\beta$  is the mixture probability, while  $\lambda_1$  and  $\lambda_2$  are the ray arrival rates.

*Remark 6:* while a delay dependence of these parameters has been conjectured, no measurements results have been found up to now to support this.

For some environments, most notably the industrial environment, a "dense" arrival of multipath components was observed, i.e., each resolvable delay bin contains significant energy. In that case, the concept of ray arrival rates loses its meaning, and a realization of the impulse response based on a tapped delay line model with regular tap spacings is to be used.

The next step is the determination of the cluster powers and cluster shapes. The power delay profile (mean power of the different paths) is exponential within each cluster

$$E\{|a_{k,l}|^2\} = \Omega_l \frac{1}{\gamma_l [(1-\beta)\lambda_1 + \beta\lambda_2 + 1]} \exp(-\tau_{k,l}/\gamma_l) \quad (19)$$

where  $\Omega_l$  is the integrated energy of the  $l$ th cluster, and  $\gamma_l$  is the intra-cluster decay time constant. Note that the normalization is an approximate one, but works for typical values of  $\lambda$  and  $\gamma$ .

*Remark 7:* Some measurements, especially in industrial environments, indicate that the first path of each cluster carries a larger mean energy than what we would expect from an exponential profile. However, due to a lack of measurements, this has not been taken into account in the final model

The cluster decay rates are found to depend linearly on the arrival time of the cluster,

$$\gamma_l \propto k_\gamma T_l + \gamma_0 \quad (20)$$

where  $k_\gamma$  describes the increase of the decay constant with delay.

The mean (over the cluster shadowing) mean (over the small-scale fading) energy (normalized to  $\gamma_l$ ), of the  $l$ th cluster follows in general an exponential decay

$$10 \log(\Omega_l) = 10 \log(\exp(-T_l/\Gamma)) + M_{cluster} \quad (21)$$

where  $M_{cluster}$  is a normally distributed variable with standard deviation  $\sigma_{cluster}$  around it.

For the NLOS case of some environments (office and industrial), the shape of the power delay profile can be different, namely (on a log-linear scale)

$$E\{|a_{k,1}|^2\} = (1 - \chi \cdot \exp(-\tau_{k,l}/\gamma_{rise})) \cdot \exp(-\tau_{k,l}/\gamma_1) \cdot \frac{\gamma_1 + \gamma_{rise}}{\gamma_1} \frac{\Omega_1}{\gamma_1 + \gamma_{rise}(1 - \chi)} \quad (22)$$

Here, the parameter  $\chi$  describes the attenuation of the first component, the parameter  $\gamma_{rise}$  determines how fast the PDP increases to its local maximum, and  $\gamma_1$  determines the decay at late times.

### E. Auxiliary parameters

The above parameters give a complete description of the power delay profile. Auxiliary parameters that are helpful in many contexts are the mean excess delay, rms delay spread, and number of multipath components that are within 10 dB of the peak amplitude. Those parameters are used only for informational purposes.

The rms delay spread is a quantity that has been used extensively in the past for the characterization of delay dispersion. It is defined as the second central moment of the PDP:

$$S_\tau = \sqrt{\frac{\int_{-\infty}^{\infty} P(\tau)\tau^2 d\tau}{\int_{-\infty}^{\infty} P(\tau)d\tau} - \left(\frac{\int_{-\infty}^{\infty} P(\tau)\tau d\tau}{\int_{-\infty}^{\infty} P(\tau)d\tau}\right)^2}. \quad (23)$$

and can thus be immediately related to the PDP as defined from the SV model. However, it is not possible to make the reverse transition, i.e., conclude about the parameters of the SV model from the rms delay spread. This quantity is therefore not considered as a basic quantity, but only as auxiliary parameter that allows better comparison with existing measurements.

It is also noticeable that the delay spread depends on the distance, as many measurement campaigns have shown. However, this effect is neglected in our channel model. The main reason for that is that it makes the simulations (e.g., coverage area) significantly simpler. As different values of the delay spread are implicit in the different environments, it is anticipated that this simplification does not have an impact on the selection, which is based on the *relative* performance of different systems anyway.

Another auxiliary parameter is the number of multipath components that is within  $x$  dB of the peak amplitude, or the number of MPCs that carries at least  $y$  % of the total energy. Those can be determined from the power delay profile in conjunction with the amplitude fading statistics (see below) and therefore are not a primary parameter.

### F. Small-scale fading

The distribution of the small-scale amplitudes is Nakagami

$$pdf(x) = \frac{2}{\Gamma(m)} \left(\frac{m}{\Omega}\right)^m x^{2m-1} \exp\left(-\frac{m}{\Omega}x^2\right), \quad (24)$$

where  $m \geq 1/2$  is the Nakagami  $m$ -factor,  $\Gamma(m)$  is the gamma function, and  $\Omega$  is the mean-square value of the amplitude. A conversion to a Rice distribution is approximately possible with the conversion equations

$$m = \frac{(K_r + 1)^2}{(2K_r + 1)} \quad (25)$$

and

$$K_r = \frac{\sqrt{m^2 - m}}{m - \sqrt{m^2 - m}}. \quad (26)$$

where  $K$  and  $m$  are the Rice factor and Nakagami- $m$  factor respectively.

The parameter  $\Omega$  corresponds to the mean power, and its delay dependence is thus given by the power delay profile above. The  $m$ -parameter is modeled as a lognormally distributed random variable, whose logarithm has a mean  $\mu_m$  and standard deviation  $\sigma_m$ . Both of these can have a delay dependence

$$\mu_m(\tau) = m_0 - k_m \tau \quad (27)$$

$$\sigma_m(\tau) = \hat{m}_0 - \hat{k}_m \tau \quad (28)$$

For the first component of each cluster, the Nakagami factor is modeled differently. It is assumed to be deterministic and independent of delay

$$m = \tilde{m}_0 \quad (29)$$

*Remark 8:* It is anticipated that also this  $m$  - factor has a mean and a variance, both of which might depend on the delay. However, sufficient data are not available.

### G. Complete list of parameters

The considered parameters are thus

- $G_0$  pathloss at 1m distance
- $n$  pathloss exponent
- $\sigma_S$  shadowing standard deviation
- $A_{\text{ant}}$  antenna loss
- $\kappa$  frequency dependence of the pathloss

- $\bar{L}$  mean number of clusters
- $\Lambda$  inter-cluster arrival rate
- $\lambda_1, \lambda_2, \beta$  ray arrival rates (mixed Poisson model parameters)
- $\Gamma$  inter-cluster decay constant
- $k_\gamma, \gamma_0$  intra-cluster decay time constant parameters
- $\sigma_{\text{cluster}}$  cluster shadowing variance
- $m_0, k_m$ , Nakagami m factor mean
- $\hat{m}_0, \hat{k}_m$ , Nakagami m factor variance
- $\tilde{m}_0$ , Nakagami m factor for strong components
- $\gamma_{\text{rise}}, \gamma_1$ , and  $\chi$  parameters for alternative PDP shape

#### H. Flow graph for the generation of impulse responses

The above specifications are a complete description of the model. In order to help a practical implementation, the following procedure suggests a "cooking recipe" for the implementation of the model:

- if the model for the specific environment has the Saleh-Valenzuela shape, proceed the following way:
  - Generate a Poisson-distributed random variable  $L$  with mean  $\bar{L}$ . This is the number of clusters for the considered realization
  - create  $L - 1$  exponentially distributed variables  $x_n$  with decay constant  $\Lambda$ . The times  $\sum_{n=1}^L x_n$  give the arrival times of the first components of each cluster
  - for each cluster, generate the cluster decay time and the total cluster power, according to equations 20 and 21, respectively.
  - for each cluster, generate a number of exponentially distributed variables  $x_n$ , from which the arrival times of the paths can be obtained. The actual number of considered components depends on the required dynamic range of the model. In the MATLAB program shown in Appendix II, it is assured that all components with a power within  $x$  dB of the peak power are included.
  - for each component, compute the mean power according to (19)
- for the office NLOS or the factory NLOS, compute the mean power according to (22); note that there are components at regularly spaced intervals that are multiples of the inverse system bandwidth.
- for each first component of the cluster, set the  $m$ -factor to  $\tilde{m}_0$ ; for industrial environments, only set  $m$ -factor of first component of first cluster to  $\tilde{m}_0$
- for all other components, compute the mean and the variance of the  $m$ -factor according to Eq. (27), (28).
- for each component, compute the realization of the amplitude as Nakagami-distributed variable with mean-square given by the mean power of the components as computed three steps above, and  $m$ -factor as computed one step above
- compute phase for each component as uniformly distributed,
- apply a filtering with a  $f^{-\kappa}$  filter.
- make sure that the above description results in a profile that has AVERAGE power 1, i.e., when averaged over all the different random processes.
- For the simulation of the actual system, multiply the transfer function of the channel with the frequency-dependent transfer function of the channel with the frequency-dependent pathloss and emission spectrum

$$P_{\text{TX-amp}}(f) \cdot \eta_{\text{TX-ant}}(f) \eta_{\text{RX-ant}}(f) \frac{G_0}{(d/d_0)^2 (f/f_c)^2} \quad (30)$$

- Note that shadowing should not be included for the simulations according to the selection criteria document.

### III. UWB MODEL PARAMETERIZATION FOR 2-10 GHz

The following parameterization was based on measurements that do not cover the full frequency range and distance range envisioned in the PAR. From a scientific point of view, the parameterization can be seen as valid only for the range over which measurement data are available. However, for the comparison purposes within the 802.15.4a group, the parameterization is used for *all* ranges.

#### A. Residential environments

The model was extracted based on measurements that cover a range from 7-20m, up to 10 GHz. The derivation and justification of the parameters can be found in document [04-452], and all measurements are included in [04-290]

Residential	LOS	NLOS
valid range of $d$	7 – 20 m	7 – 20 m
Path gain		
$G_0$ [dB]	-43.9	-48.7
$n$	1.79	4.58
$S$ [dB]	2.22	3.51
$\kappa$	$1.12 \pm 0.12$	$1.53 \pm 0.32$
Power delay profile		
$\bar{L}$	3	3.5
$\Lambda$ [1/ns]	0.047	0.12
$\lambda_1, \lambda_2$ [1/ns], $\beta$	1.54, 0.15, 0.095	1.77, 0.15, 0.045
$\Gamma$ [ns]	22.61	26.27
$k_\gamma$	0	0
$\gamma_0$ [ns]	12.53	17.50
$\sigma_{\text{cluster}}$ [dB]	2.75	2.93
Small-scale fading		
$m_0$ [dB]	0.67	0.69
$\hat{m}_0$ [dB]	0.28	0.32
$\tilde{m}_0$	NA	NA

### B. Indoor office environment

The model was extracted based on measurements that cover a range from 3-28m, 2-8 GHz. A description of the model derivation can be found in [04-383, 04-385, 04-439, 04-440, 04-447].

Office	LOS	NLOS
valid range of $d$	3 – 28 m	3 – 28 m
Path gain		
$n$	1.63	3.07
$\sigma_S$	1.9	3.9
$G_0$ [dB]	-35.4	-59.9
$\kappa$	0.03	0.71
Power delay profile		
$\bar{L}$	5.4	1
$\Lambda$ [1/ns]	0.016	NA
$\lambda_1, \lambda_2$ [1/ns], $\beta$	0.19, 2.97, 0.0184	NA
$\Gamma$ [ns]	14.6	NA
$k_\gamma$	0	NA
$\gamma_0$ [ns]	6.4	NA
$\sigma_{\text{cluster}}$ [dB]	3	NA
Small-scale fading		
$m_0$	0.42 dB	0.50 dB
$\hat{m}_0$	0.31	0.25
$\tilde{m}_0$	NA	NA
$\chi$	NA	0.86
$\gamma_{\text{rise}}$	NA	15.21
$\gamma_1$	NA	11.84

*Remark 9:* Some of the NLOS measurement points exhibited a PDP shape that followed the multi-cluster (WV) model, while others showed the first-increasing, then-decreasing shape of Eq. 22. In order to reduce the number of environments to be simulated, only the latter case was included for the NLOS environment.

### C. Outdoor environment

The model was extracted based on measurements that cover a range from 5-17m, 3-6 GHz. A description of the model derivation can be found in [04-383, 04-385, 04-439, 04-440].



Outdoor	LOS	NLOS	Farm
valid range of $d$	5 – 17 m	5 – 17 m	
Path gain			
$n$	1.76	2.5	1.58
$\sigma_S$	0.83	2	3.96
$G_0$	-45.6	-73.0	-48.96
$\kappa$	0.12	0.13	0
Power delay profile			
$\bar{L}$	13.6	10.5	3.31
$\Lambda$ [1/ns]	0.0048	0.0243	0.0305
$\lambda_1$ [1/ns]	0.27	0.15	0.0225, 0, 0
$\lambda_2$ [1/ns]	2.41	1.13	
$\beta$	0.0078	0.062	
$\Gamma$ [ns]	31.7	104.7	56
$k_\gamma$	0	0	0
$\gamma_0$ [ns]	3.7	9.3	0.92
$\sigma_{\text{cluster}}$ [dB]			3
Small-scale fading			
$m_0$	0.77 dB	0.56 dB	4.1 dB
$\hat{m}_0$	0.78	0.25	2.5 dB
$\tilde{m}_0$	NA	NA	0

The values of  $\sigma$ ,  $n$ , and  $\kappa$  for the NLOS case are "educated guesses".

#### D. Open outdoor environments

The model was extracted based on simulations of a farm area. The derivation of the model and a description of the simulations (for the farm area) can be found in [04-475].

Outdoor	Farm
valid range of $d$	
Path gain	
$n$	1.58
$\sigma_S$	3.96
$G_0$	-48.96
$\kappa$	0
Power delay profile	
$\bar{L}$	3.31
$\Lambda$ [1/ns]	0.0305
$\lambda_1$ [1/ns]	0.0225, 0, 0
$\lambda_2$ [1/ns]	
$\beta$	
$\Gamma$ [ns]	56
$k_\gamma$	0
$\gamma_0$ [ns]	0.92
$\sigma_{\text{cluster}}$ [dB]	3
Small-scale fading	
$m_0$	4.1 dB
$\hat{m}_0$	2.5 dB
$\tilde{m}_0$	0

#### E. Industrial environments

The model was extracted based on measurements that cover a range from 2 to 8 m, though the pathloss also relies on values from the literature, 3-8m. The measurements are described in [13].

Industrial	LOS	NLOS
valid range of $d$	2 – 8 m	2 – 8 m
Path gain		
$n$	1.2	2.15
$\sigma_S$ [dB]	6	6
$G_0$ [dB]	-56.7	-56.7
$\kappa$	-1.103	-1.427
Power delay profile		
$\bar{L}$	4.75	1
$\Lambda$ [1/ns]	0.0709	NA
$\lambda$ [1/ns]	NA	NA
$\Gamma$	13.47	NA
$k_\gamma$	0.926	NA
$\gamma_0$	0.651	NA
$\sigma_{\text{cluster}}$ [dB]	4.32	NA
Small-scale fading		
$m_0$	0.36 dB	0.30 dB
$\hat{m}_0$	1.13	1.15
$\tilde{m}_0$ dB	12.99	
$\chi$	NA	1
$\gamma_{\text{rise}}$ [ns]	NA	17.35
$\gamma_1$ [ns]	NA	85.36

The pathloss exponent is extracted from [14], the shadowing variance from [14], [15]. The value of  $\tilde{m}_0$  is only for the first cluster, all later components have the same mean  $m$ .

*Remark 10:* Some of the NLOS measurement points exhibited a PDP shape that followed the multi-cluster (WV) model, while others showed the first-increasing, then-decreasing shape of Eq. 22. In order to reduce the number of environments to be simulated, only the latter case was included for the NLOS environment.

#### IV. UWB MODEL PARAMETERIZATION FOR 100-1000 MHz

The channel model for the 100 – 1000 MHz case is different in its structure from the 2 – 10 GHz model. Part of the reason is that there is an insufficient number of measurements available to do a modeling that is as detailed and as realistic as the 2 – 10 GHz mode. Furthermore, only one class of environments (indoor, office-like) is available. The model is essentially the model of [16], with some minor modifications to account for a larger bandwidth considered in the downselection here.

The average PDP, i.e., the power per delay bin averaged over the small-scale fading, is exponentially decaying, except for a different power distribution in the first bin

$$\bar{G}_k = \begin{cases} \frac{\bar{G}_{\text{tot}}}{1+rF(\varepsilon)} & \text{for } k = 1 \\ \frac{\bar{G}_{\text{tot}}}{1+rF(\varepsilon)} r e^{-\frac{(\tau_k - \tau_2)}{\varepsilon}} & \text{for } k = 2, \dots, L_r, \end{cases} \quad (31)$$

where

$$F(\varepsilon) = \frac{1}{1 - \exp(-\Delta\tau/\varepsilon)}. \quad (32)$$

and  $\varepsilon$  is the decay constant that is modeled as increasing with distance (note that this is a deviation from the original model of [16])

$$\varepsilon = (d/10m)^{0.5} \cdot 40 \text{ ns} \quad (33)$$

This equation gives the same delay spread as the Cassioli model at 10m distance. The distance exponent was chosen as a compromise between the results of Cassioli (no distance dependence) and the results of [17] that showed a linear increase with distance.

The power ratio  $r = \bar{G}_2/\bar{G}_1$  indicates the amount of “extra” power (compared to the pure exponential decay law) carried in the first bin. It is also modelled as a r.v., with a distribution

$$r \sim \mathcal{N}(-4.0; 3.0). \quad (34)$$

We set the width of the observation window to  $T_d = 5 \cdot \varepsilon = L_r \cdot \Delta\tau$ . Thus, the average PDP is completely specified, according to:

$$\bar{G}(\tau) = \left\{ \delta(\tau - \tau_1) + \sum_{k=2}^{L_r} \left[ r e^{-\frac{(\tau_k - \tau_2)}{\varepsilon}} \right] \delta(\tau - \tau_k) \right\}. \quad (35)$$

Next, we consider the statistics of the small-scale fading. The probability density function of the  $G_k$  can be approximated by a Gamma distribution (i.e., the Nakagami distribution in the amplitude domain) with mean  $\bar{G}_k$  and parameter  $m_k$ .<sup>3</sup> Those  $m_k$  are themselves independent truncated Gaussian r.v.'s with parameters that depend on the delay  $\tau_k$

$$\mu_m(\tau_k) = 3.5 - \frac{\tau_k}{73}, \quad (36)$$

$$\sigma_m^2(\tau_k) = 1.84 - \frac{\tau_k}{160}, \quad (37)$$

where the units of  $\tau_k$  are nanoseconds.

Note that the  $m$ -factor was chosen identical to the measurements of the Cassioli et al. model, even though the bandwidth for which we consider the system is slightly larger than in the original model. However, there were no measurements available on which an estimate for a larger bandwidth could be based.

	NLOS	comments	
Pathloss		from [18]	
$n$	2.4		
$\sigma_S$ [dB]	5.9		
$PL_0$			
$A_{\text{ant}}$	3dB		
$\kappa$ [dB/octave]	0		
Power delay profile			
$\bar{L}$	1	The NLOS case is described by a single PDP shape	
$\Lambda$ [1/ns]	NA		
$\lambda$ [1/ns]	NA		
$\Gamma$	NA		
$k_\gamma$	NA		
$\gamma_0$	NA		
$\sigma_{\text{cluster}}$ [dB]	NA		
Small-scale fading			
$m_0$	3.5	linear scale	
$\hat{k}_m$	-1/73ns		
$\hat{m}_0$	1.84		
$\hat{k}_m$	-1/160ns	$\tau = 0.5$ if realization of $m < 0.5$	
$\hat{m}_0$ dB			
$\chi$	NA		
$\gamma_{\text{rise}}$ [ns]	NA		
$\gamma_1$ [ns]	NA		

In order to generate impulse responses at various distances, the following procedure should be used: the stored impulse responses available at the 802 server have all the same average power (with the exception of the first component, which is chosen according to the ratio  $r$ ). The proponent should then compute the decay time constant for a chosen distance  $d$  according to  $\varepsilon = (d/10m)^{0.5} \cdot 40ns$ , and attenuate the samples of the stored impulse responses with  $\exp(-\tau/\varepsilon)$ . Subsequently, the newly created impulse responses are normalized to unit total energy.

## V. BODY AREA NETWORK

Section II presented a generic channel model representing typical indoor and outdoor environments for evaluating 802.15.4a systems. However, measurements of the radio channel around the human body indicate that some modifications are necessary to accurately model a body area network (BAN) scenario. A complete description of the BAN channel parameter extraction procedure and resulting model are provided in [04-486]. This section only summarizes the most important conclusions together with the implementation and evaluation procedure. Note that the model is based on simulations with  $2GHz$  bandwidth, and *cannot* be applied to systems with larger bandwidth. Such systems should be downfiltered, in order to assess their *relative* performance in a narrower band.

### A. Model summary

Due to the extreme close range and the fact that the antennas are worn on the body, the BAN channel model has different path loss, amplitude distribution, clustering, and inter-arrival time characteristics compared with the other application scenarios within the 802.15.4a context.

<sup>3</sup>Nakagami fading channels have received considerable attention in the study of various aspects of wireless systems. A comprehensive description of the Nakagami distribution is given in [?], and the derivation and physical insights of the Nakagami-fading model can be found in [?].

Analysis of the electromagnetic field near the body using a finite difference time domain (FDTD) simulator indicated that in the 2-6 GHz range, no energy is penetrating through the body. Rather, pulses transmitted from an antenna diffract around the body and can reflect off of arms and shoulders. Thus, distances between the transmitter and receiver in our path loss model are defined as the distance *around* the perimeter of the body, rather than the straight-line distance *through* the body. In addition, the path loss mechanisms near the body are probably dominated by energy absorption from human tissue which results in an exponential decay of power versus distance.

The amplitude distributions measured near the body are also different from traditional communication environments. Since there were only a small number of multipath components that we could not resolve in our measurement, traditional Rayleigh and Ricean models are not justified and showed a very poor fit. Rather, the lognormal distribution was clearly superior. While the Nakagami-m distribution proposed for 802.15.4a can well-approximate lognormal distributions under some limited circumstances, this was not the case for the lognormal distributions observed near the body. In addition, the uncorrelated scattering assumption assumed in other models is violated for systems where both the transmitter and receiver are placed on the same body. This is not at all surprising since the multi-path components have overlapping path trajectories especially in the vicinity of the transmitter and receiver, all multipath component path lengths are very short, and there is a natural symmetry of the body.

Our measurements indicate that there are always two clusters of multi path components due to the initial wave diffracting around the body, and a reflection off of the ground. Thus, the number of clusters is always 2 and does not need to be defined as a stochastic process as in the other scenarios. Furthermore, the inter-cluster arrival times is also deterministic and depending on the exact position of the transmitters on the body. To simplify this, we have assumed a fixed average inter-cluster arrival time depending on the specified scenario.

The very short transmission distances result in small inter-ray arrival times within a cluster which are difficult to estimate without a very fine measurement resolution. Furthermore, we could not confirm if the Poisson model proposed here is valid for use around the body. Thus, these parameters are not included in our model.

Finally, the extracted channel parameters depended on the position of the receiver on the body. To incorporate this effect easily without having to perform a large number of simulations, only three scenarios are defined corresponding to a receiver placed on the ‘front’, ‘side’, and ‘back’ of the body. All channel parameters corresponding to these scenarios are summarized in section V D.

In conclusion, we recommend a body area channel model for comparing system performance for BAN scenarios consisting of the following features:

- Exponential path loss around the body
- Correlated log normal amplitude distributions
- A fixed two-cluster model
- Fixed inter-cluster arrival time
- Fixed inter-ray arrival time
- Three scenarios corresponding to the front, side and back of the body

## B. Channel Implementation Recipe

Implementing this model on a computer involves generating  $N$  correlated lognormal variables representing the  $N$  different bins, and then applying an appropriate path loss based on the distance between the antennas around the body. This can be accomplished by generating  $N$  correlated normal variables, adding the pathloss, and then converting from a dB to linear scale as follows:

$$Y_{dB} = \mathbf{X} \cdot \text{chol}(\mathbf{C}) - \mathbf{M} + G_{dB} \quad (38)$$

$\mathbf{X}$  is a vector of  $N$  uncorrelated, unit-mean, unit-variance, normal variables. To introduce the appropriate variances and cross-correlation coefficients, this vector is multiplied by the upper triangular cholesky factorization of the desired covariance matrix  $\mathbf{C}$ . The means (a vector  $\mathbf{M}$ ) of each different bin and the large scale path loss ( $G_{dB}$ ) are then introduced. The resulting vector  $Y_{dB}$  now consists of  $N$  correlated normal variables. This can be converted into the desired  $N$  correlated lognormal variables easily by transforming  $\mathbf{Y}_{dB}$  into the linear domain.

The path gain can be calculated according to the following formula:

$$G_{dB} = -\gamma(d - d_0) + G_{0,dB} \quad (39)$$

with  $\gamma$  in units of dB/meter.  $d$  is the distance between antennas,  $d_0$  is the reference distance, and  $P_0$  is the power at the reference distance. The parameters of this path loss model extracted from the simulator and measurements are also summarized in section V D for each scenario.

While this is straightforward to implement, a well-commented Matlab function [UWB\_BAN\_channel.m] is provided in the appendix to easily generate channel realizations according to this procedure to aid designers in evaluating system proposals.

### C. Evaluation Procedure

To minimize the amount of simulations that need to be performed in comparing system proposals, a simplified BAN evaluation procedure was agreed upon by the channel sub-group. Matlab code for generating test channels according to this procedure are provided in [genTestChannels.m].

Rather than evaluating the system at all of the different distances, typical transmission distances corresponding to the ‘front’, ‘side’, and ‘back’ scenarios are generated using a uniform distribution. These distances were extracted from the body used in the simulator and are summarized below:

- Front: 0.04 – 0.17 m
- Side: 0.17 – 0.38 m
- Back: 0.38 – 0.64 m

Analysis of the cluster due to the ground reflection indicated that its amplitude depended on the type of floor material. Rather than simulating for each material individually, typical floor materials (corresponding to metal, concrete, and average ground) are generated at random with equal probability in evaluating systems.

### D. BAN Channel Parameter Summary

Path loss parameters are summarized in table 1. They can be loaded into Matlab using the pathloss\_par.mat file.

Parameter	Value
$\gamma$	107.8 dB/m
$d_0$	0.1 m
$P_0$	35.5 dB

TABLE I  
PATHLOSS MODEL FOR BAN.

The covariance matrices (C) and mean vectors (M) describing the amplitude distributions of each bin are given by tables 2-3 and equation (2) in the BAN channel document [04-486]. For each scenario, these parameters can also be loaded directly into Matlab from the front\_par.mat, side\_par.mat, and back\_par.mat files. The loaded parameters Cbody and Cground provide the covariance matrices of the initial cluster and the ground reflection cluster respectively. Similarly, Mbody and Mground provide the vector of means for each cluster. It is assumed that the arrival time between the first and second cluster is 8.7 ns for the ‘front’ scenario, 8.0 ns for the ‘side’ scenario, and 7.4 ns for the ‘back’ scenario. The inter-ray arrival time is fixed to 0.5 ns.

mean and variance of lognormal distribution for BAN						
	front	front	side	side	back	back
Bin	$\mu_{dB}/2$	$\sigma_{dB}/2$	$\mu_{dB}/2$	$\sigma_{dB}/2$	$\mu_{dB}/2$	$\sigma_{dB}/2$
1	5.7	4.7	9.6	6.3	9.2	6.3
2	12.1	4.2	12.9	5.7	12.0	6.5
3	17.0	5.2	16.8	5.2	14.6	6.3
4	20.7	5.1	19.6	5.0	15.1	5.7
5	23.2	5.1	19.6	5.0	18.2	5.4
6	25.6	4.5	24.1	4.8	20.9	5.7
7	28.4	4.6	26.7	5.0	22.7	5.5
8	31.4	4.6	28.9	5.0	23.9	5.2
9	34.5	4.8	30.9	5.2	24.0	5.1
10	37.1	4.7	32.4	5.6	24.9	5.4

1 0.9 0.78 0.77 0.73 0.64 0.62 0.53 0.53 0.45  
 0.9 1 0.88 0.83 0.77 0.74 0.72 0.64 0.64 0.59  
 0.78 0.88 1 0.84 0.76 0.77 0.76 0.7 0.69 0.66  
 0.77 0.83 0.84 1 0.86 0.81 0.81 0.74 0.75 0.73  
 0.73 0.77 0.76 0.86 1 0.85 0.83 0.74 0.72 0.69  
 0.64 0.74 0.77 0.81 0.85 1 0.92 0.81 0.75 0.72  
 0.62 0.72 0.76 0.81 0.83 0.92 1 0.86 0.81 0.77  
 0.53 0.64 0.70 0.74 0.74 0.81 0.86 1 0.92 0.86  
 0.53 0.64 0.69 0.75 0.72 0.75 0.81 0.92 1 0.91  
 0.45 0.59 0.66 0.73 0.69 0.72 0.77 0.86 0.91 1  
 Correlation values for side arrangement  
 1 0.86 0.56 0.66 0.66 0.51

0.86 1 0.74 0.74 0.73 0.59  
 0.56 0.74 1 0.82 0.79 0.71  
 0.66 0.74 0.82 1 0.87 0.62  
 0.66 0.73 0.79 0.87 1 0.76  
 0.51 0.59 0.71 0.62 0.76 1

Correlation values for front arrangement

1 0.88 0.84 0.78 0.55 0.59 0.54 0.48 0.62 0.72  
 0.88 1 0.91 0.76 0.70 0.74 0.63 0.57 0.71 0.81  
 0.84 0.91 1 0.81 0.68 0.80 0.72 0.63 0.74 0.81  
 0.78 0.76 0.81 1 0.69 0.69 0.79 0.68 0.69 0.70  
 0.55 0.70 0.68 0.69 1 0.83 0.76 0.84 0.82 0.82  
 0.59 0.74 0.80 0.69 0.83 1 0.85 0.84 0.83 0.81  
 0.54 0.63 0.72 0.79 0.76 0.85 1 0.86 0.77 0.71  
 0.48 0.57 0.63 0.68 0.84 0.84 0.86 1 0.85 0.77  
 0.62 0.71 0.74 0.69 0.82 0.83 0.77 0.85 1 0.91  
 0.72 0.81 0.81 0.70 0.82 0.81 0.71 0.77 0.91 1

correlation values for back arrangement

## VI. CHANNEL MODEL FOR 1MHZ CARRIER FREQUENCY

### A. Pathloss

This section will discuss the pathloss for traditional far field links and summarize the differences between far field and near field links. Then, this section will introduce a near field link equation that provides path loss for low frequency near field links. Note that the pathloss model for the 1 MHz range is a narrowband model, so that the conventional definitions of pathloss can be used. The definitions below require the definitions of antenna gains, which have to be specified by the proponents. However, in contrast to the UWB case, the gain is not frequency dependent. Examples for achievable values as a function of the size can be found in the last part of this section.

The relationship between transmitted power ( $P_{TX}$ ) and received power ( $P_{RX}$ ) in a far-field RF link is given by "Friis's Law:"

$$G(f, d) = \frac{P_{RX}}{P_{TX}} = \frac{G_{TX}G_{RX}\lambda^2}{(4\pi)^2 d^2} = \frac{G_{TX}G_{RX}}{4} \frac{1}{(kd)^2} \quad (40)$$

where  $G_{TX}$  is the transmit antenna gain,  $G_{RX}$  is the receive antenna gain,  $\lambda$  is the RF wavelength,  $k = 2\pi/\lambda$  is the wave number, and  $d$  is the distance between the transmitter and receiver. In other words, the far-field power rolls off as the inverse square of the distance ( $1/d^2$ ). Near-field links do not obey this relationship. Near field power rolls off as powers higher than inverse square, typically inverse fourth ( $1/d^4$ ) or higher.

This near field behavior has several important consequences. First, the available power in a near field link will tend to be much higher than would be predicted from the usual far-field, Friis's Law relationship. This means a higher signal-to-noise ratio (SNR) and a better performing link. Second, because the near-fields have such a rapid roll-off, range tends to be relatively finite and limited. Thus, a near-field system is less likely to interfere with another RF system outside the operational range of the near-field system.

Electric and magnetic fields behave differently in the near field, and thus require different link equations. Reception of an electric field signal requires an electric antenna, like a whip or a dipole. Reception of a magnetic field signal requires a magnetic antenna, like a loop or a loopstick. The received signal power from a co-polarized electric antenna is proportional to the time average value of the incident electric field squared:

$$P_{RX(E)} \sim \langle |\mathbf{E}|^2 \rangle \sim \left( \frac{1}{(kd)^2} - \frac{1}{(kd)^4} + \frac{1}{(kd)^6} \right), \quad (41)$$

for the case of a small electric dipole transmit antenna radiating in the azimuthal plane and being received by a vertically polarized electric antenna. Similarly, the received signal power from a co-polarized magnetic antenna is proportional to the time average value of the incident magnetic field squared:

$$P_{RX(H)} \sim \langle |\mathbf{H}|^2 \rangle \sim \left( \frac{1}{(kd)^2} + \frac{1}{(kd)^4} \right). \quad (42)$$

Thus, the "near field" pathloss formulas are:

$$G_E(d, f) = \frac{P_{RX(E)}}{P_{TX}} = \frac{G_{TX}G_{RX(E)}}{4} \left( \frac{1}{(kd)^2} - \frac{1}{(kd)^4} + \frac{1}{(kd)^6} \right) \quad (43)$$

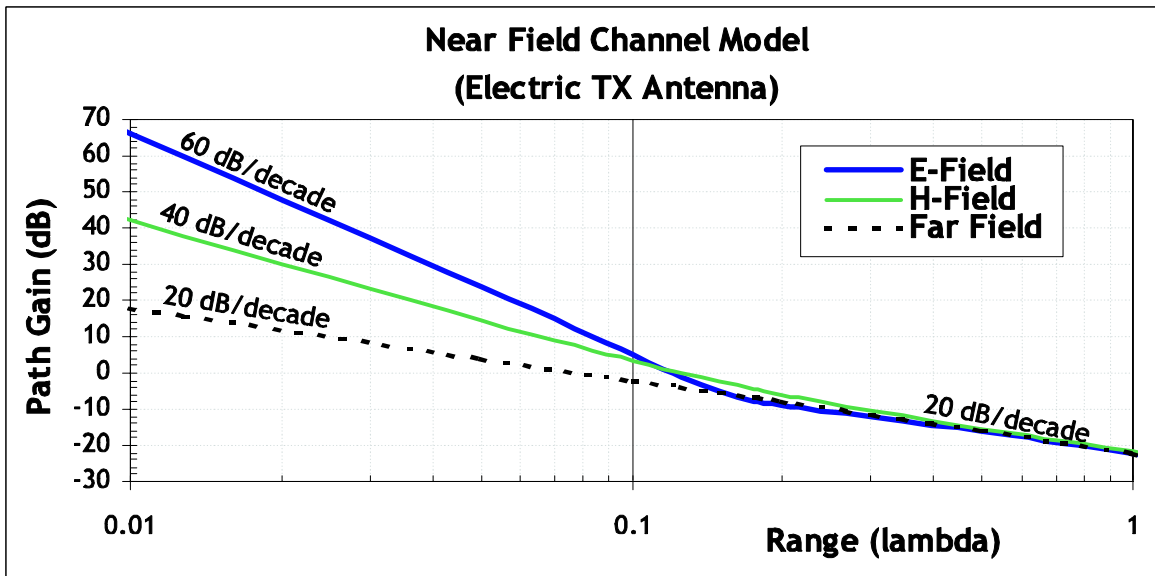


Fig. 1. Behavior of typical near field channel.

for the electric field signal, and:

$$G_H(d, f) = \frac{P_{RX(H)}}{P_{TX}} = \frac{G_{TX}G_{RX}}{4} \left( \frac{1}{(kr)^2} + \frac{1}{(kr)^4} \right) \quad (44)$$

for the magnetic field signal. At a typical near field link distance where  $kd \cong 1$  ( $d \cong \lambda/2\pi$ ), a good approximation is:

$$G(d, f) \cong \frac{1}{4} G_{TX}G_{RX}. \quad (45)$$

In other words, the typical pathloss in a near field channel is on the order of  $-6$  dB. At very short ranges, pathloss may be on the order of 60 dB or more. At an extreme range of about one wavelength the pathloss may be about 18 dB. This behavior is summarized in the figure below:

Experimental data showing the accuracy of a near field ranging system is available elsewhere.<sup>4</sup>

### B. Near Field Phase Equations

The near field phase behavior was derived elsewhere.<sup>5</sup> For an electric transmit antenna, the magnetic phase is:

$$\phi_H = -\frac{180}{\pi} [kr + (\cot^{-1} kr + n\pi)], \quad (46)$$

and the electric phase varies as:

$$\phi_E = -\frac{180}{\pi} \left\{ kr + \left[ \cot^{-1} \left( kr - \frac{1}{kr} \right) + n\pi \right] \right\}. \quad (47)$$

### C. Attenuation and Delay Spread:

The near field link and phase equations above describe free space links. In practice, the free space formulas provide an excellent approximation to propagation in an open field environment. In heavily cluttered environments, signals may be subject to additional attenuation or enhancement. Attenuation or enhancement of signals may be included to match measured data. Even in heavily cluttered environments, low frequency near field signals are rarely attenuated or enhanced by more than about 20 dB. In most typical indoor propagation environments, results are comparable to free space results and attenuation or enhancement are not necessary for an accurate model. The key complication introduced by the indoor environment is phase distortions caused by the delay spread of multipath.

<sup>4</sup>Kai Siwiak, "Near Field Electromagnetic Ranging," IEEE802.15-04/0360r0, 13 July 2004.

<sup>5</sup>Hans Schantz, "Near Field Ranging Algorithm," IEEE802.15-04/0438r0, 17 August 2004.

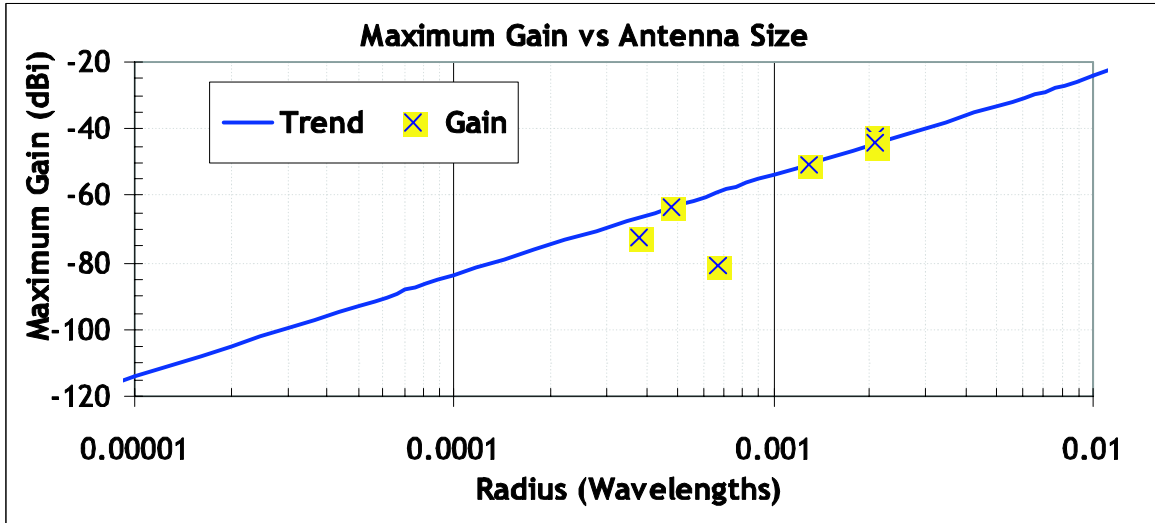


Fig. 2. Gain vs Size for Selected Electrically Small Antennas

The concept of a delay spread is not directly applicable to a near field channel because the wavelength of a low frequency near field system is much longer than the propagation environment. Instead, a near field channel in a complex propagation environment is characterized by phase distortions that depend upon the echo response of the environment. Since this echo response is largely insensitive to frequency, delay spread measurements at higher frequencies provide an excellent indication of the phase deviation magnitude to expect at lower frequencies.

In propagation testing of near field systems indoors, typical delay deviations are on the order of  $\tau_{RMS} = 30\text{-}50$  ns, consistent with what might be expected for a microwave link. For instance, a system operating at 1 MHz with an RF period of  $1\ \mu\text{s}$  will experience phase deviations of 11–18 degrees. The worst case near field delay observed to date has been an outlier on the order of 100 ns corresponding to a 36 degree deviation at 1 MHz.

The delay spread tends to be distance dependent:<sup>6</sup>

$$\tau_{RMS} = \tau_0 \sqrt{\frac{d}{d_0}}, \quad (48)$$

where  $d$  is the distance,  $d_0 = 1$  m is the reference distance, and the delay spread parameter is  $\tau_0 = 5.5$  ns.<sup>7</sup> In the limit where the RMS delay spread is much smaller than the period of the signals in questions, the RMS phase variation is:

$$\phi_{RMS} = \omega \tau_{RMS} = 2\pi f \tau_{RMS}, \quad (49)$$

where  $f$  is the operational frequency. Thus, a good model for phase behavior is to add a normally distributed phase perturbation with zero mean and a standard deviation equal to the RMS delay spread. Thus:

$$\phi_H = -\frac{180}{\pi} [kr + (\cot^{-1} kr + n\pi)] + Norm[0, \phi_{RMS}] \quad (50)$$

and

$$\phi_E = -\frac{180}{\pi} \left\{ kr + \left[ \cot^{-1} \left( kr - \frac{1}{kr} \right) + n\pi \right] \right\} + Norm[0, \phi_{RMS}] \quad (51)$$

In summary, to a reasonable approximation, signal power in a near field link follows from the free space model. Further, one may assume that the delay spread as measured at microwave frequencies is typical of the phase deviation to be expected at low frequencies.

#### D. Antenna Size vs Performance:

For the above equations, it is necessary to include the This section presents some results from antennas constructed by the Q-Track Corporation. The figure below shows gain vs. size for Q-Track's antennas as well as a trend line.

For instance at the 1.3 MHz frequency used by Q-Track's prototype antenna, a typical receive antenna occupies a boundary sphere of radius 11 cm and has a gain of -63.6 dB. A typical transmit antenna is a thin wire whip occupying a boundary sphere of radius 30 cm and having a gain of -51 dB.

<sup>6</sup>Kai Siwiak et al, "On the relation between multipath and wave propagation attenuation," Electronic Letters, 9 January 2003 Vol. 39, No. 1, pp. 142-143.

<sup>7</sup>Kai Siwiak, "UWB Channel Model for under 1 GHz," IEEE 802.15-04/505r0, 10 October, 2004.



### E. Implementation recipe

The recipe for the implementation of the model is thus the following:

- Establish the distance between transmitter and receiver,  $d$ , as well as the wavenumber  $k$
- From this, determine the value of the rms delay spread from Eq. (48);
- Compute the phases of E and H field from Eq. (51) and (50), using Eq. (49)
- Determine the received power of the E and H field from Eq. (60) and Eq. (44), using the values for the antenna efficiencies used by the proposer; to get the signal amplitude as the square root of that value.
- Multiply the amplitude with the phase to get the (scalar) value of the impulse response in E and H field

Note that also this model does not include any correlation between the realizations of the impulse response at different locations.

## VII. SUMMARY AND CONCLUSIONS

This document has presented channel models for the evaluation of IEEE 802.15.4a system proposals. The models are completely specified, and MATLAB programs for the implementation are given in the appendix for the convenience of the user

### APPENDIX I

#### SUMMARY OF ALL CONTRIBUTIONS

##### A. Abstract for documents about measurement procedure and the extraction of parameters

Ref. [04-283] describes a unified measurement procedure and methods to extract channel parameters from measurement data. It forms the basis for part of the appendix of the final report (measurement procedure, extraction of large-scale parameters and the SV model parameters).

##### B. Measurements in residential environments

Document [04-112] by Haneda et al. from CRL describes the results of spatio-temporal propagation channel measurements in a typical home environments in Japan. In the delay domain, cluster spreads on the order of 1.5ns are observed. Also, angular characteristics are described.

Chong et al. made extensive measurements in indoor residential environment. Measurements were conducted in several types of high-rise apartments based in several cities in Korea. Ref. [04-282] consists of detailed characterization of the path loss and temporal-domain parameters of the UWB channel with bandwidth from 3 to 10 GHz. Document [04-306] contains the measurement procedure in more detail. Ref. [04-290] gives an overview of the parameterization of residential environments, including a literature overview. [04-452] describes an update and most recent version of the model.

##### C. Abstract for office and outdoor measurements

The IEEE 15.4a channel modeling subcommittee has been assigned with the task of coming out with channel models for various UWB environments in order to evaluate the ALT-PHY proposals for IEEE 802.15.4a applications. Various institutes and industries who are members of this channel modeling subcommittee have done extensive channel measurements for different UWB propagation environments. The channel modeling subcommittee agreed to adopt the S-V model with minor modifications.

As part of the channel modeling subcommittee, Institute for Infocomm Research, A\*STAR, Singapore has also done extensive UWB measurements to characterize the indoor office and outdoor UWB propagation environments. The measurement and parameter extraction procedures for both Indoor office and outdoor environments are reported in [04-383, 04-385, 04-439, and 04-440].

From this measurements campaign, we concluded that the amplitudes can be best modeled by Nakagami distributions, where the m-factor follows a log-normal distribution. In the S-V model, ray arrival is modeled by a single Poisson process. However, we showed in [04-385] that the ray arrival process can be better modeled by mixture of Poisson processes.

The presentation [04-447] describes UWB channel measurements from 2 GHz to 8 GHz in the frequency domain, conducted in two office buildings at ETH Zurich, Switzerland. Measurements were taken for LOS, OLOS and NLOS settings in a corridor and a large lobby, with transmitter-receiver separations ranging from 8 m to 28m. The focus of the measurements was to establish a model suitable for theoretical analysis, but we also used the measured data to extract the IEEE 802.15.4a standard model parameters as presented in this document. We use a model selection approach to conclude that tap amplitude statistics are adequately described by the Rayleigh distribution in most cases, while the lognormal model as used by the IEEE 802.15.3a working group shows a consistently bad fit.

##### D. Abstracts for Body Area Networks

Fort et al. present details of a model for body area networks in a series of documents. Document [P802.15-04-486-00-004a] is the final model that contains the details of the simulations and other aspects of the derivation of the model, as well as details in the implementation of a MATLAB program. It forms the basis for the BAN model in the final report and the MATLAB program given in the appendix. Several other documents describe preliminary versions of this, including [04-120], [04-371].

### E. Abstracts for Open Area environments

[04-215] by Emami et al. describes an ultra-wideband channel model for open area/farm applications. The channel model is based on ray tracing that captures signal descriptors including frequencies. The rationale behind the channel model is developed and presented in support of the presentation. [325] and [475] give updated versions.

[04-449] by Keignart and Daniele describes the measurement campaign done in a snow covered environment. From this campaign path loss exponent and a simple propagation model have been extracted.

### F. Pathloss models

Document [04-111] from Sato and Kobayashi describes a new line-of-sight path loss formula for ultra wideband signals in the presence of the ground plane reflection.

In [04-408], Siwiak shows a basic two slope propagation attenuation model, which can be used in conjunction with a multipath channel description

### G. Low-frequency models

[04-417] presents a theoretical analysis of the near field channel in free space. Then this document offers a reasonable strawman channel model for purposes of comparison of near field location systems: (1) Assume attenuation no worse than 20 dB below the free space near field channel model and (2) Assume phase deviations consistent with the delay spread measured at microwave frequencies

### H. Status reports and summaries of minutes of meetings

A number of documents contain intermediate administrative information, like status reports to the full group, collection of minutes of phones conferences, etc. These documents have the numbers 04-024 (status Januar 04), 04-195 (status March); 04-346 (status July), telemeetings are summarized in [04-204] (Nov. 03 March 04), [04-345] (April - July 2004),

## APPENDIX II

### MATLAB PROGRAM FOR GENERATION OF IMPULSE RESPONSES

#### A. MATLAB program for "normal" UWB environments

```
% modified S-V channel model evaluation
%
% Written by Sun Xu, Kim Chee Wee, B. Kannan & Francois Chin on 22/02/2005
clear;
no_output_files = 1; % non-zero: avoids writing output files of continuous-time responses
num_channels = 100; % number of channel impulse responses to generate
randn('state',12); % initialize state of function for repeatability
rand('state',12); % initialize state of function for repeatability
cm_num = 6; % channel model number from 1 to 8
% get channel model params based on this channel model number
[Lam,Lmean,lambda_mode,lambda_1,lambda_2,beta,Gam,gamma_0,Kgamma, ...
sigma_cluster,nlos,gamma_rise,gamma_1,chi,m0,Km,sigma_m0,sigma_Km, ...
sfading_mode,m0_sp,std_shdw,kappa,fc,fs] = uwb_sv_params_15_4a( cm_num );
fprintf(1,['Model Parameters\n' ...
'Lam = %.4f, Lmean = %.4f, lambda_mode(FLAG) = %d\n' ...
'lambda_1 = %.4f, lambda_2 = %.4f, beta = %.4f\n' ...
'Gam = %.4f, gamma0 = %.4f, Kgamma = %.4f, sigma_cluster = %.4f\n' ...
'nlos(FLAG) = %d, gamma_rise = %.4f, gamma_1 = %.4f, chi = %.4f\n' ...
'm0 = %.4f, Km = %.4f, sigma_m0 = %.4f, sigma_Km = %.4f\n' ...
'sfading_mode(FLAG) = %d, m0_sp = %.4f, std_shdw = %.4f\n', ...
'kappa = %.4f, fc = %.4fGHz, fs = %.4fGHz\n'], ...
Lam,Lmean,lambda_mode,lambda_1,lambda_2,beta,Gam,gamma_0,Kgamma, ...
sigma_cluster,nlos,gamma_rise,gamma_1,chi,m0,Km,sigma_m0,sigma_Km,...
sfading_mode,m0_sp,std_shdw,kappa,fc,fs);
ts = 1/fs; % sampling frequency
% get a bunch of realizations (impulse responses)
[h_ct,t_ct,t0,np] = uwb_sv_model_ct_15_4a(Lam,Lmean,lambda_mode,lambda_1, ...
lambda_2,beta,Gam,gamma_0,Kgamma,sigma_cluster,nlos,gamma_rise,gamma_1, ...
chi,m0,Km,sigma_m0,sigma_Km,sfading_mode,m0_sp,std_shdw,num_channels,ts);
```

```

% change to complex baseband channel
h_ct_len = size(h_ct, 1);
phi = zeros(h_ct_len, 1);
for k = 1:num_channels
phi = rand(h_ct_len, 1).*(2*pi);
h_ct(:,k) = h_ct(:,k) .* exp(phi .* i);
end
% now reduce continuous-time result to a discrete-time result
[hN,N] = uwb_sv_cnvt_ct_15_4a( h_ct, t_ct, np, num_channels, ts );
if N > 1,
h = resample(hN, 1, N); % decimate the columns of hN by factor N
else
h = hN;
end
% add the frequency dependency
[h]= uwb_sv_freq_depend_ct_15_4a(h,fc,fs,num_channels,kappa);
%*****
% Testing and plotting
%*****
% channel energy
channel_energy = sum(abs(h).^2);
h_len = length(h(:,1));
t = [0:(h_len-1)] * ts; % for use in computing excess & RMS delays
excess_delay = zeros(1,num_channels);
RMS_delay = zeros(1,num_channels);
num_sig_paths = zeros(1,num_channels);
num_sig_e_paths = zeros(1,num_channels);
for k=1:num_channels
% determine excess delay and RMS delay
sq_h = abs(h(:,k)).^2 / channel_energy(k);
t_norm = t - t0(k); % remove the randomized arrival time of first cluster
excess_delay(k) = t_norm * sq_h;
RMS_delay(k) = sqrt( ((t_norm-excess_delay(k)).^2) * sq_h );
% determine number of significant paths (paths within 10 dB from peak)
threshold_dB = -10; % dB
temp_h = abs(h(:,k));
temp_thresh = 10^(threshold_dB/20) * max(temp_h);
num_sig_paths(k) = sum(temp_h > temp_thresh);
% determine number of sig. paths (captures x % of energy in channel)
x = 0.85;
temp_sort = sort(temp_h.^2); % sorted in ascending order of energy
cum_energy = cumsum(temp_sort(end:-1:1)); % cumulative energy
index_e = min(find(cum_energy >= x * cum_energy(end)));
num_sig_e_paths(k) = index_e;
end
energy_mean = mean(10*log10(channel_energy));
energy_stddev = std(10*log10(channel_energy));
mean_excess_delay = mean(excess_delay);
mean_RMS_delay = mean(RMS_delay);
mean_sig_paths = mean(num_sig_paths);
mean_sig_e_paths = mean(num_sig_e_paths);
fprintf(1,'Model Characteristics\n');
fprintf(1,' Mean delays: excess (tau_m) = %.1f ns, RMS (tau_rms) = %.1f\n', ...
mean_excess_delay, mean_RMS_delay);
fprintf(1,' # paths: NP_10dB = %.1f, NP_85%% = %.1f\n', ...
mean_sig_paths, mean_sig_e_paths);
fprintf(1,' Channel energy: mean = %.1f dB, std deviation = %.1f dB\n', ...
energy_mean, energy_stddev);

```

```

figure(1); clf; plot(t, abs(h)); grid on
title('Impulse response realizations')
xlabel('Time (nS)')
figure(2); clf; plot([1:num_channels], excess_delay, 'b-', ...
[1 num_channels], mean_excess_delay*[1 1], 'r-');
grid on
title('Excess delay (nS)')
xlabel('Channel number')
figure(3); clf; plot([1:num_channels], RMS_delay, 'b-', ...
[1 num_channels], mean_RMS_delay*[1 1], 'r-');
grid on
title('RMS delay (nS)')
xlabel('Channel number')
figure(4); clf; plot([1:num_channels], num_sig_paths, 'b-', ...
[1 num_channels], mean_sig_paths*[1 1], 'r-');
grid on
title('Number of significant paths within 10 dB of peak')
xlabel('Channel number')
figure(5); clf; plot([1:num_channels], num_sig_e_paths, 'b-', ...
[1 num_channels], mean_sig_e_paths*[1 1], 'r-');
grid on
title('Number of significant paths capturing > 85% energy')
xlabel('Channel number')
temp_average_power = sum((abs(h))'.*(abs(h))', 1)/num_channels;
temp_average_power = temp_average_power/max(temp_average_power);
average_decay_profile_dB = 10*log10(temp_average_power);
threshold_dB = -40;
above_threshold = find(average_decay_profile_dB > threshold_dB);
ave_t = t(above_threshold);
apdf_dB = average_decay_profile_dB(above_threshold);
figure(6); clf; plot(ave_t, apdf_dB); grid on
title('Average Power Decay Profile')
xlabel('Delay (nsec)')
ylabel('Average power (dB)')
if no_output_files,
return
end
%*****
%Saving the data
%*****
%% save continuous-time (time,value) pairs to files
save_fn = sprintf('cm%d_imr', cm_num);
% A complete self-contained file for Matlab users
save([save_fn '.mat'], 't', 'h', 't_ct', 'h_ct', 't0', 'np', 'num_channels', 'cm_num');
% Three comma-delimited text files for non-Matlab users:
% File #1: cmX_imr_np.csv lists the number of paths in each realization
dlmwrite([save_fn '_np.csv'], np, ','); % number of paths
% File #2: cmX_imr_ct.csv can open with Excel
% n'th pair of columns contains the (time,value) pairs for the n'th realization
% save continuous time data
th_ct = zeros(size(t_ct,1),3*size(t_ct,2));
th_ct(:,1:3:end) = t_ct; % time
th_ct(:,2:3:end) = abs(h_ct); % magnitude
th_ct(:,3:3:end) = angle(h_ct); % phase (radians)
fid = fopen([save_fn '_ct.csv'], 'w');
if fid < 0,
error('unable to write .csv file for impulse response, file may be open in another application');
end

```

```

for k = 1:size(th_ct,1)
fprintf(fid,'%0.4f,%0.6f', th_ct(k,1:end-2));
fprintf(fid,'%0.4f,%0.6f\r\n', th_ct(k,end-1:end)); % \r\n for Windoze end-of-line
end
fclose(fid);
% File #3: cmX_imr_dt.csv can open with Excel
% discrete channel impulse response magnitude and phase pair realization.
% the first column is time. phase is in radians
% save discrete time data
th = zeros(size(h,1),2*size(h,2)+1);
th(:,1) = t'; % the first column is time scale
th(:,2:2:end) = abs(h); % even columns are magnitude
th(:,3:2:end) = angle(h); % odd columns are phase
fid = fopen([save_fn '_dt.csv'], 'w');
if fid < 0,
error('unable to write .csv file for impulse response, file may be open in another application');
end
for k = 1:size(th,1)
fprintf(fid,'%0.4f,%0.6f', th(k,1:end-2));
fprintf(fid,'%0.4f,%0.6f\r\n', th(k,end-1:end)); % \r\n for Windoze end-of-line
end
fclose(fid);
return; % end of program

```

```

function [Lam,Lmean,lambda_mode,lambda_1,lambda_2,beta,Gam,gamma_0,Kgamma, ...
sigma_cluster,nlos,gamma_rise,gamma_1,chi,m0,Km,sigma_m0,sigma_Km, ...
sfading_mode,m0_sp,std_shdw,kappa,fc,fs] = uwb_sv_params_15_4a( cm_num )
% Written by Sun Xu, Kim Chee Wee, B. Kannan & Francois Chin on 22/02/2004
% Return modified S-V model parameters for standard UWB channel models
%_____
% Lam Cluster arrival rate (clusters per nsec)
% Lmean Mean number of Clusters
% lambda_mode Flag for Mixture of poisson processes for ray arrival times
% 1 -> Mixture of poisson processes for the ray arrival times
% 2 -> tapped delay line model
% lambda_1 Ray arrival rate for Mixture of poisson processes (rays per nsec)
% lambda_2 Ray arrival rate for Mixture of poisson processes (rays per nsec)
% beta Mixture probability
%_____
% Gam Cluster decay factor (time constant, nsec)
% gamma0 Ray decay factor (time constant, nsec)
% Kgamma Time dependence of ray decay factor
% sigma_cluster Standard deviation of normally distributed variable for cluster energy
% nlos Flag for non line of sight channel
% 0 -> LOS
% 1 -> NLOS with first arrival path starting at t ~ 0
% 2 -> NLOS with first arrival path starting at t = 0 and diffused first cluster
% gamma_rise Ray decay factor of diffused first cluster (time constant, nsec)
% gamma_1 Ray decay factor of diffused first cluster (time constant, nsec)
% chi Diffuse weight of diffused first cluster
%_____
% m0 Mean of log-normal distributed nakagami-m factor
% Km Time dependence of m0
% sigma_m0 Standard deviation of log-normal distributed nakagami-m factor
% sigma_Km Time dependence of sigma_m0
% sfading_mode Flag for small-scale fading
% 0 -> All paths have same m-factor distribution
% 1 -> LOS first path has a deterministic large m-factor

```

```

% 2 -> LOS first path of each cluster has a deterministic
% large m-factor
% m0_sp Deterministic large m-factor
% _____
% std_shdw Standard deviation of log-normal shadowing of entire impulse response
% _____
% kappa Frequency dependency of the channel
% _____
% fc Center Frequency
% fs Frequency Range
%
% modified by I2R
if cm_num == 1, % Residential LOS
% MPC arrival
Lam = 0.047; Lmean = 3;
lambda_mode = 1;
lambda_1 = 1.54; lambda_2 = 0.15; beta = 0.095;
% MPC decay
Gam = 22.61; gamma_0 = 12.53; Kgamma = 0; sigma_cluster = 2.75;
nlos = 0;
gamma_rise = NaN; gamma_1 = NaN; chi = NaN; % dummy in this scenario
% Small-scale Fading
m0 = 0.67; Km = 0; sigma_m0 = 0.28; sigma_Km = 0;
sfading_mode = 0; m0_sp = NaN;
% Large-scale Fading – Shadowing
std_shdw = 2.22;
% Frequency Dependence
kappa = 1.12;
fc = 6; % GHz
fs = 8; % 2 - 10 GHz
elseif cm_num == 2, % Residential NLOS
% MPC arrival
Lam = 0.12; Lmean = 3.5;
lambda_mode = 1;
lambda_1 = 1.77; lambda_2 = 0.15; beta = 0.045;
% MPC decay
Gam = 26.27; gamma_0 = 17.5; Kgamma = 0; sigma_cluster = 2.93;
nlos = 1;
gamma_rise = NaN; gamma_1 = NaN; chi = NaN; % dummy in this scenario
% Small-scale Fading
m0 = 0.69; Km = 0; sigma_m0 = 0.32; sigma_Km = 0;
sfading_mode = 0; m0_sp = NaN;
% Large-scale Fading – Shadowing
std_shdw = 3.51;
% Frequency Dependence
kappa = 1.53;
fc = 6; % GHz
fs = 8; % 2 - 10 GHz
elseif cm_num == 3, % Office LOS
% MPC arrival
Lam = 0.016; Lmean = 5.4;
lambda_mode = 1;
lambda_1 = 0.19; lambda_2 = 2.97; beta = 0.0184;
% MPC decay
Gam = 14.6; gamma_0 = 6.4; Kgamma = 0; sigma_cluster = 3; % assumption
nlos = 0;
gamma_rise = NaN; gamma_1 = NaN; chi = NaN; % dummy in this scenario
% Small-scale Fading

```

```

m0 = 0.42; Km = 0; sigma_m0 = 0.31; sigma_Km = 0;
sfading_mode = 2; m0_sp = 3; % assumption
% Large-scale Fading – Shadowing
std_shdw = 0; %1.9;
% Frequency Dependence
kappa = 0.03;
fc = 6; % GHz
fs = 8; % 3 - 6 GHz
elseif cm_num == 4, % Office NLOS
% MPC arrival
Lam = 0.19; Lmean = 3.1;
lambda_mode = 1;
lambda_1 = 0.11; lambda_2 = 2.09; beta = 0.0096;
% MPC decay
Gam = 19.8; gamma_0 = 11.2; Kgamma = 0; sigma_cluster = 3; % assumption
nlos = 2;
gamma_rise = 15.21; gamma_1 = 11.84; chi = 0.78;
% Small-scale Fading
m0 = 0.5; Km = 0; sigma_m0 = 0.25; sigma_Km = 0;
sfading_mode = 0; m0_sp = NaN; % assumption
% Large-scale Fading – Shadowing
std_shdw = 3.9;
% Frequency Dependence
kappa = 0.71;
fc = 6; % GHz
fs = 8; % 3 - 6 GHz
elseif cm_num == 5, % Outdoor LOS
% MPC arrival
Lam = 0.0448; Lmean = 13.6;
lambda_mode = 1;
lambda_1 = 0.13; lambda_2 = 2.41; beta = 0.0078;
% MPC decay
Gam = 31.7; gamma_0 = 3.7; Kgamma = 0; sigma_cluster = 3; % assumption
nlos = 0;
gamma_rise = NaN; gamma_1 = NaN; chi = NaN; % dummy in this scenario
% Small-scale Fading
m0 = 0.77; Km = 0; sigma_m0 = 0.78; sigma_Km = 0;
sfading_mode = 2; m0_sp = 3; % assumption
% Large-scale Fading – Shadowing
std_shdw = 0.83;
% Frequency Dependence
kappa = 0.12;
fc = 6; % GHz
fs = 8; % 3 - 6 GHz
elseif cm_num == 6, % Outdoor NLOS
% MPC arrival
Lam = 0.0243; Lmean = 10.5;
lambda_mode = 1;
lambda_1 = 0.15; lambda_2 = 1.13; beta = 0.062;
% MPC decay
Gam = 104.7; gamma_0 = 9.3; Kgamma = 0; sigma_cluster = 3; % assumption
nlos = 1;
gamma_rise = NaN; gamma_1 = NaN; chi = NaN; % dummy in this scenario
% Small-scale Fading
m0 = 0.56; Km = 0; sigma_m0 = 0.25; sigma_Km = 0;
sfading_mode = 0; m0_sp = NaN; % assumption
% Large-scale Fading – Shadowing
std_shdw = 2; % assumption

```

```

% Frequency Dependence
kappa = 0.13;
fc = 6; % GHz
fs = 8; % 3 - 6 GHz
elseif cm_num == 7, % Industrial LOS
% MPC arrival
Lam = 0.0709; Lmean = 4.75;
lambda_mode = 2;
lambda_1 = 1; lambda_2 = 1; beta = 1; % dummy in this scenario
% MPC decay
Gam = 13.47; gamma_0 = 0.615; Kgamma = 0.926; sigma_cluster = 4.32;
nlos = 0;
gamma_rise = NaN; gamma_1 = NaN; chi = NaN; % dummy in this scenario
% Small-scale Fading
m0 = 0.36; Km = 0; sigma_m0 = 1.13; sigma_Km = 0;
sfading_mode = 1; m0_sp = 12.99;
% Large-scale Fading – Shadowing
std_shdw = 6;
% Frequency Dependence
kappa = -1.103;
fc = 6; % GHz
fs = 8; % 2 - 8 GHz
elseif cm_num == 8, % Industrial NLOS
% MPC arrival
Lam = 0.089; Lmean = 1;
lambda_mode = 2;
lambda_1 = 1; lambda_2 = 1; beta = 1; % dummy in this scenario
% MPC decay
Gam = 5.83; gamma_0 = 0.3; Kgamma = 0.44; sigma_cluster = 2.88;
nlos = 2;
gamma_rise = 47.23; gamma_1 = 84.15; chi = 0.99;
% Small-scale Fading
m0 = 0.3; Km = 0; sigma_m0 = 1.15; sigma_Km = 0;
sfading_mode = 0; m0_sp = NaN; % m0_sp is assumption
% Large-scale Fading – Shadowing
std_shdw = 6;
% Frequency Dependence
kappa = -1.427;
fc = 6; % GHz
fs = 8; % 2 - 8 GHz
elseif cm_num == 9, % Open Outdoor Environment NLOS (Fram, Snow-Covered Open Area)
% MPC arrival
Lam = 0.0305; Lmean = 3.31;
lambda_mode = 1;
lambda_1 = 0.0225; lambda_2 = 1; beta = 1;
% MPC decay
Gam = 56; gamma_0 = 0.92; Kgamma = 0; sigma_cluster = 3; % sigma_cluster is assumption
nlos = 1;
gamma_rise = NaN; gamma_1 = NaN; chi = NaN;
% Small-scale Fading
m0 = 4.1; Km = 0; sigma_m0 = 2.5; sigma_Km = 0;
sfading_mode = 0; m0_sp = NaN; % m0_sp is assumption
% Large-scale Fading – Shadowing
std_shdw = 3.96;
% Frequency Dependence
kappa = -1; % Kappa is assumption
fc = 6; % GHz
fs = 8; % 2 - 8 GHz

```



```

else
error('cm_num is wrong!!')
end
return

function [h]= uwb_sv_freq_depend_ct_15_4a(h,fc,fs,num_channels,kappa)
% This function is used to include the frequency dependency
f0 = 5; % GHz
h_len = length(h(:,1));
f = [fc-fs/2 : fs/h_len/2 : fc+fs/2]./f0;
f = f.^(-2*(kappa));
f = [f(h_len : 2*h_len), f(1 : h_len-1)]';
i = (-1)^(1/2); % complex i
for c = 1:num_channels
% add the frequency dependency
h2 = zeros(2*h_len, 1);
h2(1 : h_len) = h(:,c); % zero padding
fh2 = fft(h2);
fh2 = fh2 .* f;
h2 = ifft(fh2);
h(:,c) = h2(1:h_len);
% Normalize the channel energy to 1
h(:,c) = h(:,c)/sqrt(h(:,c)' * h(:,c) );
end
return
function [h,t,t0,np] = uwb_sv_model_ct_15_4a(Lam,Lmean,lambda_mode,lambda_1, ...
lambda_2,beta,Gam,gamma_0,Kgamma,sigma_cluster,nlos,gamma_rise,gamma_1, ...
chi,m0,Km,sigma_m0,sigma_Km,sfading_mode,m0_sp,std_shdw,num_channels,ts)
% Written by Sun Xu, Kim Chee Wee, B. Kannan & Francois Chin on 22/02/2005
% IEEE 802.15.4a UWB channel model for PHY proposal evaluation
% continuous-time realization of modified S-V channel model
% Input parameters:
% detailed introduction of input parameters is at uwb_sv_params.m
% num_channels number of random realizations to generate
% Outputs
% h is returned as a matrix with num_channels columns, each column
% holding a random realization of the channel model (an impulse response)
% t is organized as h, but holds the time instances (in nsec) of the paths whose
% signed amplitudes are stored in h
% t0 is the arrival time of the first cluster for each realization
% np is the number of paths for each realization.
% Thus, the k'th realization of the channel impulse response is the sequence
% of (time,value) pairs given by (t(1:np(k),k), h(1:np(k),k))
%
% modified by I2R
% initialize and precompute some things
std_L = 1/sqrt(2*Lam); % std dev (nsec) of cluster arrival spacing
std_lam_1 = 1/sqrt(2*lambda_1);
std_lam_2 = 1/sqrt(2*lambda_2);
% std_lam = 1/sqrt(2*lambda); % std dev (nsec) of ray arrival spacing
h_len = 1000; % there must be a better estimate of # of paths than this
ngrow = 1000; % amount to grow data structure if more paths are needed
h = zeros(h_len,num_channels);
t = zeros(h_len,num_channels);
t0 = zeros(1,num_channels);
np = zeros(1,num_channels);
for k = 1:num_channels % loop over number of channels
tmp_h = zeros(size(h,1),1);

```

```

tmp_t = zeros(size(h,1),1);
if nlos == 1,
Tc = (std_L*randn)^2 + (std_L*randn)^2; % First cluster random arrival
else
Tc = 0; % First cluster arrival occurs at time 0
end
t0(k) = Tc;
if nlos == 2 & lambda_mode == 2
L = 1; % for industrial NLOS environment
else
L = max(1, poisrnd(Lmean)); % number of clusters
end
%%%%%%%%%%%%%%%%%%%%%%%%%%%%%%%%%%%%%%%%%%%%%%%%%%%%%%%%%%%%%%%%%%%%%%%%
if Kgamma ~= 0 & nlos == 0
Tcval = []; Tc_cluster = [];
Tc_cluster(1,1) = Tc;
for i_Tc = 2:L+1
Tc_cluster(1,i_Tc) = Tc_cluster(1,i_Tc-1) + (std_L*randn)^2 + (std_L*randn)^2;
end
end
%%%%%%%%%%%%%%%%%%%%%%%%%%%%%%%%%%%%%%%%%%%%%%%%%%%%%%%%%%%%%%%%%%%%%%%%
cluster_index = zeros(1,L);
path_ix = 0;
nak_m = [];
for ncluster = 1:L
% Determine Ray arrivals for each cluster
Tr = 0; % first ray arrival defined to be time 0 relative to cluster
cluster_index(ncluster) = path_ix + 1; % remember the cluster location
gamma = Kgamma*Tc + gamma_0; % delay dependent cluster decay time
if nlos == 2 & ncluster == 1
gamma = gamma_1;
end
Mcluster = sigma_cluster*randn;
Pcluster = 10*log10(exp(-1*Tc/Gam)) + Mcluster; % total cluster power
Pcluster = 10^(Pcluster*0.1);
%%%%%%%%%%%%%%%%%%%%%%%%%%%%%%%%%%%%%%%%%%%%%%%%%%%%%%%%%%%%%%%%%%%%%%%%
if Kgamma ~= 0 & nlos == 0
Tr_len = Tc_cluster(1,ncluster+1) - Tc_cluster(1,ncluster);
else
Tr_len = 10*gamma;
end
%%%%%%%%%%%%%%%%%%%%%%%%%%%%%%%%%%%%%%%%%%%%%%%%%%%%%%%%%%%%%%%%%%%%%%%%
while (Tr < Tr_len),
t_val = (Tc+Tr); % time of arrival of this ray
if nlos == 2 & ncluster == 1
% equation (22)
h_val = Pcluster*(1-chi*exp(-Tr/gamma_rise))*exp(-Tr/gamma_1) ...
*(gamma+gamma_rise)/gamma/(gamma+gamma_rise*(1-chi));
else
% equation (19)
h_val = Pcluster/gamma*exp(-Tr/gamma)/(beta*lambda_1+(1-beta)*lambda_2+1);
end
path_ix = path_ix + 1; % row index of this ray
if path_ix > h_len,
% grow the output structures to handle more paths as needed
tmp_h = [tmp_h; zeros(ngrow,1)];
tmp_t = [tmp_t; zeros(ngrow,1)];
h = [h; zeros(ngrow,num_channels)];

```

```

t = [t; zeros(ngrow,num_channels)];
h_len = h_len + ngrow;
end
tmp_h(path_ix) = h_val;
tmp_t(path_ix) = t_val;
% if lambda_mode == 0
% Tr = Tr + (std_lam*randn)^2 + (std_lam*randn)^2;
if lambda_mode == 1
if rand < beta
Tr = Tr + (std_lam_1*randn)^2 + (std_lam_1*randn)^2;
else
Tr = Tr + (std_lam_2*randn)^2 + (std_lam_2*randn)^2;
end
elseif lambda_mode == 2
Tr = Tr + ts;
else
error('lambda mode is wrong!')
end
% generate log-normal distributed nakagami m-factor
m_mu = m0 - Km*t_val;
m_std = sigma_m0 - sigma_Km*t_val;
nak_m = [nak_m, lognrnd(m_mu, m_std)];
end
Tc = Tc + (std_L*randn)^2 + (std_L*randn)^2;
%%%%%%%%%%%%%%%%%%%%%%%%%%%%%%%%%%%%%%%%%%%%%%%%%%%%%%%%%%%%%%%%%%%%%%%%
if Kgamma ~= 0 & nlos == 0
Tc = Tc_cluster(1,ncluster+1);
end
%%%%%%%%%%%%%%%%%%%%%%%%%%%%%%%%%%%%%%%%%%%%%%%%%%%%%%%%%%%%%%%%%%%%%%%%
end
% change m value of the first multipath to be the deterministic value
if sfading_mode == 1
nak_ms(cluster_index(1)) = m0_sp;
elseif sfading_mode == 2
nak_ms(cluster_index) = m0_sp;
end
% apply nakagami
for path = 1:path_ix
h_val = (gamrnd(nak_m(path), tmp_h(path)/nak_m(path))).^(1/2);
tmp_h(path) = h_val;
end
np(k) = path_ix; % number of rays (or paths) for this realization
[sort_tmp_t,sort_ix] = sort(tmp_t(1:np(k))); % sort in ascending time order
t(1:np(k),k) = sort_tmp_t;
h(1:np(k),k) = tmp_h(sort_ix(1:np(k)));
% now impose a log-normal shadowing on this realization
% fac = 10^(std_shdw*randn/20) / sqrt( h(1:np(k),k)' * h(1:np(k),k) );
% h(1:np(k),k) = h(1:np(k),k) * fac;
end
return

function [hN,N] = uwb_sv_cnvrct_ct_15_4a( h_ct, t, np, num_channels, ts )
% convert continuous-time channel model h_ct to N-times oversampled discrete-time samples
% h_ct, t, np, and num_channels are as specified in uwb_sv_model
% ts is the desired time resolution
%
% hN will be produced with time resolution ts / N.
% It is up to the user to then apply any filtering and/or complex downconversion and then

```

```

% decimate by N to finally obtain an impulse response at time resolution ts.
min_Nfs = 100; % GHz
N = max( 1, ceil(min_Nfs*ts) ); % N*fs = N/ts is the intermediate sampling frequency before decimation
N = 2^nextpow2(N); % make N a power of 2 to facilitate efficient multi-stage decimation
Nfs = N / ts;
t_max = max(t(:)); % maximum time value across all channels
h_len = 1 + floor(t_max * Nfs); % number of time samples at resolution ts / N
hN = zeros(h_len,num_channels);
for k = 1:num_channels
    np_k = np(k); % number of paths in this channel
    t_Nfs = 1 + floor(t(1:np_k,k) * Nfs); % vector of quantized time indices for this channel
    for n = 1:np_k
        hN(t_Nfs(n),k) = hN(t_Nfs(n),k) + h_ct(n,k);
    end
end
end

```

### B. MATLAB program for body area networks

```

function h = UWB_BAN_channel_v2(N,d,position,floor)
%
% Written by Andrew Fort (IMEC, Belgium. September 29, 2004)
%
% PROTOTYPE
%
% h = UWB_BAN_channel_v2(N,d,position,floor)
%
% INPUTS
%
% N = number of channels to generate
% d = distance between tx and rx (meters)
% position = Position on body ('front','side','back')
% floor = Material of floor ('PEC' (perfect electrical conductor),
% 'concrete', average 'ground', or 'none')
%
% OUTPUTS
%
% h = N randomly generated channel responses
%
% DESCRIPTION
%
% h is an N by M matrix. N is the number of different
% randomly generated channel response. M is the number of filter taps in
% a single channel realization. Taps are always separated by 0.25 ns.
%
% Results were determined empirically using a sophisticated finite difference
% time domain simulation and an anatomically correct body area model.
% General model parameters were confirmed through actual measurements.
% Load empirically derived path loss model
% P0 = reference path loss (dB)
% d0 = reference distance (m)
% m = decay rate (dB/m)
load pathloss_par.mat;
% Load empirically derived amplitude distributions
% Mbody = Mean amplitude for each bin (initial cluster)
% Cbody = Covariance matrix for each bin (initial cluster)
% Mground = Mean amplitude for each bin (ground reflection cluster)
% Cground = Covariance matrix for each bin (ground reflection cluster)
% body_ground_iat = Average inter arrival time between body and ground clusters (s)
% binlen = length of one bin (s)

```

```

switch(position)
case 'front'
load front_par.mat;
case 'side'
load side_par.mat;
case 'back'
load back_par.mat;
otherwise
error('Position parameter must be "front", "side", or "back"');
end
% The channel model is created in the log domain and then
% converted to the linear domain.
% Generate correlated normal variables representing each bin
% in the initial cluster of components diffracting around the body.
hbody = randn(N,size(Cbody,2));
hbody = hbody*chol(Cbody) + repmat(Mbody,size(hbody,1),1);
% Apply path loss model around body.
hbody = hbody + (P0 + m*(d-d0));
% Generate correlated normal variables representing each bin
% in the second cluster of components reflecting off of the ground.
% Then adjust for different kinds of floor materials
hground = randn(N,size(Cground,2));
hground = hground*chol(Cground) + repmat(Mground,size(hground,1),1) + P0;
switch(floor)
case 'PEC'
; % No adjustment needed
case 'concrete'
hground = hground + 6.0; % 6 dB adjustment due to reflection loss
case 'ground'
hground = hground + 1.1; % 1.1 dB adjustment due to reflection loss
case 'none'
hground = zeros(size(hground)) + inf; % Set this cluster of components to 0
otherwise
error('The floor argument must be "PEC", "concrete", "ground", or "none"');
end
% In general, the time of arrival of the second cluster depends on the
% heights of the antennas on the torso, and the position around the body.
% To simplify this, we used the average time between the first and second
% clusters, body_ground_iat, extracted along the front, side, and back
% of the body.
% Calculate number of bins between first and second cluster
icbin = round(body_ground_iat/binlen)-size(hbody,2);
% Create matrix of channels in the correct size:
% N by (Length of first cluster + icbin + length of second cluster)
h = zeros(N,size(hbody,2) + icbin + size(hground,2));
% Convert from dB to linear, and put the body and ground
% clusters at the correct times.
h(:,1:size(hbody,2)) = 10.^(-hbody./10);
h(:,size(hbody,2) + icbin + 1:end) = 10.^(-hground./10);
% Convert to tap amplitudes and apply uniform random phase
h = sqrt(h).*exp(j*2*pi*rand(size(h)));
function [h, d, floor] = genTestChannels(N,scenario)
% PROTOTYPE
%
% [h d floor] = genTestChannels(N,scenario)
%
% INPUTS
%
```

```

% N = number of channel realizations to generate
% scenario = 'front' of body, 'side' of body, and 'back' of body.
%
% OUTPUTS
%
% h = N by M Matrix. N = number of channel realizations. M = number of
% taps in each channel realization. Taps are separated by 0.5 ns.
% d = N by 1 matrix. Randomly generated distances for each channel
% realization.
% floor = N by 1 cell matrix. Randomly generated floor material for
% each channel realization (Either 'PEC', average 'ground', or
% 'concrete').
%
% DESCRIPTION
%
% Generates N random channels representing propagation conditions for the
% given scenario (Either 'front' of body, 'side' of body, or 'back' of
% body). Channels are realized by randomly generating appropriate distances
% and floor materials corresponding to the given scenario.
%
% Additional parameters 'd' and 'floor' describe the distance and floor
% conditions for each randomly generated channel in 'h'. Only the channel
% realizations in 'h' are needed for evaluation.
% Check parameters
N = round(N);
if(nargin < 2)
error('genTestChannels expects 2 arguments');
elseif(~isnumeric(N) | (N <= 0) )
error('N must be an integer greater than 0');
elseif(~ischar(scenario))
error('Scenario must be a string');
end
% Reset random number generator.
rand('state',sum(100*clock));
% Generate random distances
d = genDistance(N,scenario);
% Generate random floor materials
floor = genFloorMaterial(N);
% Generate random channels
for k = 1:N
h(k,:) = UWB_BAN_channel(1,d(k),scenario,floor{k});
end
% ***** SUB-FUNCTIONS *****
% Generate uniform random distances for specified scenario
function d = genDistance(N,scenario)
% Reasonable distances for transmitting around the body when the
% transmitter is placed on either the front, side, or back.
switch(scenario)
case 'front'
mindistance = 0.04;
maxdistance = 0.17;
case 'side'
mindistance = 0.17;
maxdistance = 0.38;
case 'back'
mindistance = 0.38;
maxdistance = 0.65;
otherwise

```

```

error('Scenario must be "front", "side", or "back"');
end
% Generate random distances between mindistance and maxdistance
d = zeros(N,1);
d = rand(N,1)*(maxdistance-mindistance) + mindistance;
% Generate random floor material
% Either a best case (perfect electrical conductor), intermediate
% case (average ground), or worst case (concrete).
function floor = genFloorMaterial(N)
pick = rand(N,1);
PECndx = find(pick <= 1/3);
groundndx = find((pick <= 2/3) & (pick > 1/3));
concretendx = find((pick <= 1) & (pick > 2/3));
floor = cell(N,1);
floor(PECndx) = {'PEC'};
floor(groundndx) = {'ground'};
floor(concretendx) = {'concrete'};

```

The required MAT files front\_par.mat, side\_par.mat, and back\_par.mat have been put onto the server in a zip file.

### APPENDIX III RECOMMENDATIONS FOR MEASUREMENT PROCEDURE

This appendix gives recommendations for the performance of measurements, and the extraction of data. Most of these procedures have been followed in the course of the establishment of the model, though some of them were established only after many of the measurements have been performed. In any case, this part of the documentation is only informative.

#### A. Measurement procedure

Multipath profiles are to be measured at various locations, so that the statistics can be determined. We have to distinguish four different scales:

1) *Small-scale fading*: In order to determine this, a sufficient number of measurement points has to be taken in an area where large-scale parameters like shadowing are identical. Experience shows that some 50 measurement points per area are a minimum. the measurement point must be spaced  $\lambda/2$  or more apart, to allow the measurement points to experience independent fading (though for a small angular spread, this is not guaranteed with this spacing). The

different realizations of the channel can be achieved by moving either the TX and/or the RX. Note that if the measurements are done in the 100-1000 MHz range, it might be difficult to fit 50 measurement points into a small-scale area when only one of the link ends is moved. It is also important that the statistics within the measurement area are stationary. For example, the situation should not occur where one measurement point has a LOS, while another is shadowed behind an obstacle.

2) *Large-scale fading*: Different areas within one building should be measured, that are far enough apart that large-scale propagation processes (including shadowing) are different from area to area. However, the absolute distance between TX and RX should be the same for the different areas.

Large-scale areas with different distances between TX and RX should be measured.

Variations from building to building should be measured.

The statistics for all of the different scales should be extracted. When measurements of the angular spectra are also desired, this complicates the situation. The reason for this is the different requirement for the spacing of the (small-scale) measurement points. For the extraction of the small-scale statistics, we want the measurement points as far apart as possible - at a minimum,  $\lambda/2$  for the *lowest* involved frequency. For the determination of the angular spectra, we need the measurement points no farther apart than  $\lambda/2$  for the *highest* involved frequency. The main emphasis of the measurements for the 4a channel model will lie on the small-scale statistics, not on angular spectra.

3) *Parameters that must be determined*:

- Frequency range
- Number of frequency points
- Number of array elements
- Array element spacing
- Transmit power
- Number of measurement points
- IF bandwidth
- Estimated runtime for one measurement

#### 4) Equipment:

- Network analyser
- Spectrum analyser (to check interference level)
- (At least) 2 HF antenna cables of desired length — with calibration (attenuation) curves
- 2 antennas — with calibration curves
- 2 virtual arrays — with stepper motors
- 2 tripods of the same (achievable) height
- Maps — with lengths, scale and material information
- Pre-determined measurement positions, marked on the map

## APPENDIX IV MODELING CONSIDERATIONS AND PARAMETER EXTRACTION

### A. Linear Time-Varying Systems

Modeling Radio channels is a complicated task. The complexity of the solution to Maxwell's equations needs to be reduced to a couple of parameters and some mathematically amenable formulas. The two most important steps towards this goal are the assumption of a linear channel and the description by stochastic methods. Linearity follows from Maxwell's theory as long as the materials are linear. This is a good assumption in general. A stochastic description helps to overcome the complexity of the real propagation environment. The tradeoff here is between the optimal utilization of site-specific propagation features and system robustness. A system designed with full knowledge of the propagation conditions at a certain site would be able to exploit these conditions, resulting in superior performance, whereas a system design based on a stochastic channel model will only achieve average performance — but it will achieve this performance at a wide variety of sites whereas the former will not.

1) *The System Functions:* The most general description within the framework outlined is thus a stochastic linear time-varying (LTV) system. In a classical paper, Bello [19] derived the canonical representation in terms of system functions. The input-output relation is described by the two-dimensional linear operator with kernel  $h_0(t, t')$  as<sup>8</sup>

$$y(t) = (\mathbb{H}x)(t) = \int h_0(t, t')x(t')dt'. \quad (52)$$

The kernel represents the response of the system at time  $t$  to a unit impulse launched at time  $t'$ . A more convenient representation for the following derivations can be obtained by changing the time origin<sup>9</sup>:  $h(t, \tau) = h_0(t, t - \tau)$ , representing the response of the system at time  $t$  to a unit impulse launched  $\tau$  seconds earlier. This representation is commonly referred to as the *time-varying impulse response*. The input-output relation now reads

$$y(t) = \int h(t, \tau)x(t - \tau)d\tau. \quad (53)$$

Equivalent representations can be obtained by Fourier transforms of the time-varying impulse response.  $L_{\mathbb{H}}(t, f)$

2) *Stochastic Characterization:* For a stochastic description, the system functions are modeled as random processes. A complete characterization via associated joint distributions is far too complicated to be of practical interest, hence the description is normally confined to first and second order statistics. If the processes are Gaussian and the channel hence Rayleigh fading, a second order description is indeed a complete statistical characterization. According to the four equivalent system functions, there are four equivalent correlation functions  $R_h(t, t', \tau, \tau')$

The WSS assumption is generally accepted, at least locally over a reasonable time frame. If shadowing effects come into play, the overall channel is of course no longer WSS. The US assumption however needs to be questioned for UWB channels since it is obvious that channel correlation properties change with frequency. One solution to this problem is to separate the nonstationary behavior from the small scale fading, as for example proposed by Kunisch and Pamp [21]; another possibility is the use of local scattering functions as proposed by Matz [22].

3) *UWB Channel Models:* The system functions do not depend on the bandwidth and are thus readily applicable to UWB channels. The correlation functions however only contain all statistical information if the channel process is assumed Gaussian. The notion of an infinite continuum of scatterers is approximately satisfied for narrowband channels since many reflections are not resolvable and hence the superposition of many arrivals justifies the invocation of the central limit theorem. In real world UWB channels, the number of scatterers does not necessarily scale linearly with the bandwidth and the Gaussian assumption becomes questionable due to insufficient averaging.

In narrowband channels, a model often used is a tapped delay line expression, where the channel impulse response is described as [23]

$$h(t, t') = \sum_{i=1}^{N(t')} c_i(t)\delta(t' - \tau_i(t))e^{j\theta_i(t)}. \quad (54)$$

<sup>8</sup>Unless otherwise indicated, integrals are from  $-\infty$  to  $+\infty$ .

<sup>9</sup>The following choice of the time origin is just one possibility. For an in depth discussion see the report by Artés et al. [20]



$N(\tau)$  is the number of multipath components,  $c_i(t)$  the time-varying amplitude,  $\tau_i(t)$  the time-varying path delay and  $\theta_i(t)$  the time-varying phase. The underlying assumption here is that each arrival can be associated with a single propagation path, like in a ray-tracing model. This is no longer true for UWB channels since diffraction and dispersion leads to a frequency dependent distortion of every echo. One way to get around this problem is to include linear filters in every path, as in the paper by Qiu [24]. The other possibility is to continue using a tapped delay-line model but dispose of the physical intuition relating distinct paths to channel taps and consider the tapped delay line model just as the standard discretization of a bandlimited random process without ascribe any physical meaning to the individual terms.

4) *VNA Channel Measurements*: Because of the wide bandwidth, UWB channel measurements have been performed predominantly in the frequency domain using a vector network analyzer (VNA) [21, 25–29]. Because the sweep time is quite long, the channel has to remain stationary throughout the whole measurement, practically precluding the sounding of time-variant channels. It is thus sufficient to consider a time invariant channel model with impulse response  $h(\tau)$  and frequency response  $H(f)$ . This measurement approach hence naturally leads to a time invariant model. Since it is still considered stochastic and described by appropriate distributions, the resulting simulation can only serve for packet based transmission, where during the transmission of one packet the channel remains virtually constant and changes to an independent realization for the next packet. Any algorithms making use of channel variations like channel tracking cannot be evaluated with this model.

The VNA samples the channel at different frequencies. However, the measurement points returned are not true samples of the channel transfer function.

a) *VNA Measurement System response*: An idealized VNA transmits a sinusoid for a fixed amount of time according to  $x(t) = 2g_T(t) \cos 2\pi kFt$  where  $g_T$  is a time-windowing function modeling the limited sample time,  $F$  is the frequency step size and  $k$  indicates the current measurement point. In the frequency domain, the transmitted signal is thus

$$X(f) = G_T(f - kF) + G_T(f + kF) \quad (55)$$

The channel output as measured at the receiving end is given by

$$V(f) = (G_T(f - kF) + G_T(f + kF)) H(f) \quad (56)$$

The VNA filters the signal with an RF prefilter of bandwidth  $(-B_{RF}/2, B_{RF}/2)$  and baseband equivalent transfer function  $G_{RF}(f)$ , to obtain  $Y_{RF}(f)$

## B. Extraction of large-scale parameters

This section describes the more general case where the pathloss exponent and the shadowing variance are treated as random variables. The case where they are considered as deterministic variables follows as a special case.

Unlike the narrow band case, it has been observed that the path loss in an UWB system depends on both distance ( $d$ ) and frequency ( $f$ ). This frequency dependency will complicate the large-scale parameter extraction procedure. However, it has been reported in [9] that if we consider a spatially averaged data instead of a single snap shot, this frequency dependency can be removed. Thus in this document, we will use the spatially averaged data to extract the large-scale parameters.

In [9], it was observed that the path loss exponent,  $\gamma$  and the standard deviation of the shadowing component,  $\sigma$  varied from one building to another and therefore, they were modeled by random variables as shown below:

$$\gamma = \mu\lambda + \sigma\lambda n_1 \quad (57)$$

$$\sigma = \mu\sigma + \sigma\sigma n_3 \quad (58)$$

where  $n_1$  and  $n_3$  are zero mean, unit variance Gaussian random variables. Now the path loss can be written as

$$\begin{aligned} \overline{G}(d) &= G_0 + 10\mu\lambda \log 10(d) + 10\sigma\lambda n_1 \log 10(d) + n_2\mu\sigma + n_2n_3\sigma\sigma \\ \overline{G}(d) - G_0 &= 10\mu\lambda \log 10(d) + 10\sigma\lambda n_1 \log 10(d) + n_2\mu\sigma + n_2n_3\sigma\sigma \end{aligned} \quad (59)$$

where  $n_3$  is zero mean, unit variance Gaussian random variable and  $G_0$  denotes the path loss at a reference distance.

As one can see from (59), we have 4 large-scale parameters to be extracted. At a fixed distance,  $d$  the first term in (59) is a constant (median path loss) and the last three terms together have a random variation about the median path loss. As explained in [9], these last three terms can be approximated as zero mean Gaussian variate with standard deviation of  $\sigma_{var}$ , where

$$\sigma_{var} = \sqrt{100\sigma_\gamma^2(\log_{10} d)^2 + \mu_\sigma^2 + \sigma_\sigma^2} \quad (60)$$

In this case, we need to extract only two parameters:  $\mu\lambda$  and  $\sigma_{var}$ . From the above arguments, we can see that at fixed distance  $d$ ,  $(\overline{G}(d) - G_0)$  is a Gaussian random variate with mean,  $10\mu\lambda \log 10(d)$  and standard deviation  $\sigma_{var}$ .

*How to get these parameters?*

- From the frequency domain responses at different homes/rooms, get the spatially averaged path loss,  $\overline{G}(d)$  at various distances.
- Plot the  $10 \log_{10}(\overline{G}(d)-G_0)$  vs  $10 \log_{10}(d)$  and apply the linear regression fit.
- From the gradient, calculate  $\mu\lambda$ . Square root of the second central moment will give the  $\sigma_{var}$ .
- Verify the validity of Gaussian variate assumption by comparing the empirical c.d.f. and the theoretical Gaussian c.d.f.

*What about the other parameters  $\sigma\lambda$ ,  $\mu\sigma$  and  $\sigma\sigma$ ?*

As we have explained earlier,  $\gamma$  varies with from building to building and  $\sigma$  varies from location to location. One way to extract these parameters is to obtain the  $\gamma$  and  $\sigma$  over various buildings and locations and then calculate the respective means ( $\mu\sigma, \mu\lambda$ ) and the variances ( $\sigma\sigma, \sigma\lambda$ ).

### C. Extraction of SV parameters

We consider the SV model as defined in Chapter 2 of the main text.

1) *Data Post-Processing:* Since the measurement system measured the “radio channel” (i.e. including the effect of amplifiers, cables and antennas), in order to remove these hardware effects, all raw data are normalized with the calibration data so that only the “propagation channel” data will be used for further analysis. For measurements conducted using VNA, the CTFs are transformed into the CIRs through inverse Fourier transform (IFT). Frequency domain windowing is applied prior to the transformation to reduce the leakage problem. Then, the CIRs are analyzed by divided the temporal axis into small intervals (or delay bins),  $\Delta\tau$ . This delay bin is corresponding to the width of a path and is determined by the reciprocal of the bandwidth swept (i.e. time resolution of the measurement system). The CIRs are then normalized such that the total power in each power delay profile (PDP),  $P(\tau)$  is equal to one. A cutoff threshold of 20 dB below the strongest path was applied to the PDP so that any paths arrived below his threshold is set to zero. This is to ensure that only the effective paths are used for the channel modeling. The initial delay for each of the transmission links was extracted from the PDP. This value was removed from the results so that all PDPs can be aligned with first path arrives at 0 ns.

2) *Cluster Identification:* The first task is to identify clusters. Different researchers have different definitions of a cluster. The position and the size of the clusters will be heavily dependent on the superstructure and physical layout of the considered environments. However, clustering identification employing statistical techniques such as clustering algorithms are inappropriate for this application as it is very difficult to develop a robust algorithm for the automatic identification of cluster regions. Thus, cluster regions were selected manually by visual inspection.

3) *Arrival Statistics:* In order to analyze the statistics of the clustering effects, the clusters in each data set must be identified. With the times and amplitudes of all major arrivals identified, as well as their clustering patterns, the data could be used to analyze the statistics and arrive at a model. As shown in Section II, there are 5 key parameters that define the S-V model:

- $\Lambda$  is the cluster arrival rate
- $\lambda$  is the ray arrival rate, i.e. the arrival rate of path within each cluster
- $\Gamma$  is the cluster exponential decay factor
- $\gamma$  is the ray exponential decay factor
- $\sigma$  is the standard deviation of the lognormal fading term (dB)

Following [30], the above parameters can be found using “brute force search” by trying to fit the measurement data to match different important characteristics of the channel. The main characteristics of the channel that are used to derive the above model parameters are the following:

- Mean excess delay,  $\tau_m$
- rms delay spread,  $\tau_{rms}$
- Number of MPCs within 20 dB threshold,  $NP_{20dB}$ .

Following the methodology in [31], firstly, the cluster and ray decay time constants,  $\Gamma$  and  $\gamma$ , were estimated by superimposing clusters with normalized amplitudes and time delays and selecting a mean decay rate. For example, in order to estimate  $\Gamma$ , the first cluster arrival in each set was normalized to an amplitude of one and a time delay of zero. All cluster arrivals were superimposed and plotted on a semi-logarithmic plot. The estimate for  $\Gamma$  was found by curve fitting the line (representing an exponential curve) such that the mean squared error was minimized. Similarly, in order to estimate  $\gamma$ , the first arrival in each cluster was set to a time of zero and amplitude of one, and all other ray arrivals were then adjusted accordingly and superimposed. Following this model, the best fit exponential distributions were determined from the cluster and ray arrival times, respectively. In order to estimate the Poisson cluster arrival rate,  $\Lambda$  the first arrival in each cluster was considered to be the beginning of the cluster, regardless of whether or not it had the largest amplitude. The arrival time of each cluster was subtracted from its successor, so that the conditional probability distribution given in (17) could be estimated. The Poisson ray arrival rate,  $\lambda$  was guessed based on the average separation time between arrivals. Estimates for  $\Lambda$  and  $\lambda$  were both done by fitting the sample pdf to the corresponding probability for each bin. The fitting was done using a least mean square criterion.

For the case of overlapping clusters, procedure as proposed in [32] is adopted. By assuming that each cluster has an exponential shape, a straight-line extrapolation function (in dB) is deployed on the first cluster and then subtract the PDP of the first cluster

from the total PDP. Then, the next non-overlapping region is used to extract the decay factor for the next cluster. This process is repeated for all clusters in the total PDP until the last cluster is reached. Note that the powers of overlapping rays are calculated so that the total sum of the powers of overlapping rays corresponding to different clusters equals to the powers of the original total PDP. More details of this procedure is reported in [32].

4) *Channel Tap Distribution*: The central limit theorem does not necessarily hold for UWB channels since there might not be enough unresolvable arrivals. It is thus important to characterize the distribution of the channel taps. The samples measured by the VNA are not ideal, hence any statement about densities and distributions of these VNA samples does not necessarily carry over to the original physical channel. If the channel process can be modeled as Gaussian, then the VNA samples will also be Gaussian. However, since the VNA samples are a smoothed version of the channel frequency response, they might still appear Gaussian due to the inherent averaging, even if the channel frequency response can no longer be described by a Gaussian process. In addition to the averaging effect, the receiver noise is always present, adding another Gaussian component. Hence to get close to the original channel, the baseband bandwidth  $B_{BB}$  should be chosen as small as practically possible, and high SNR conditions should always be ensured.

5) *Testing Distributions*: The tap gain distribution commonly refers to the distribution of the tap magnitude. Because the phase undergoes rapid changes whenever the path distance changes by more than a fraction of a wavelength, the standard assumption is a uniform phase distribution. For UWB signals with lower frequency bound over 1 GHz, this assumption still seems to be valid, hence in the following I will focus on the distribution of the  $|y[n_r]|$  only.

The empirical probability density function (PDF) and cumulative distribution function (CDF) of a measured channel tap  $|y[n_r]|$  can be obtained from the histogram, provided that a sufficient number of independent samples is available. Estimating the true distribution however is more a philosophical problem as to be of practical interest, since the concept of a true distribution drawn from which samples are observed, requires a probability model within which to operate. Hence the notion of a single true distribution is not relevant — the goal is to find a model that is supported by the measured data and at the same time amenable for analytical and simulation use. The goal is then to test a certain number of predefined mathematical models against the data. The choice of candidate PDFs in this case is based on experience and mathematical convenience. The more degrees of freedom a PDF has the better the fit in general, but the higher the complexity. Thus the right way to proceed is not to find the model with the best fit but the model attaining a prescribed goodness of fit with the least complexity. Typical candidate PDFs for mobile radio channels are Rayleigh, Rice, Nakagami, Gamma, Lognormal and to a lesser extent Weibull. This is a *model selection problem*, and several methods were developed by statisticians starting with the work of Akaike in the early 1970s [33]. Among the established criteria for model selection are the Akaike information Criterion (AIC), the Bayesian information Criterion (BIC) and the principle of minimum description length (MDL).

Surprisingly, these model selection techniques are hardly ever used in the field of channel modeling. Instead most researchers rely on *hypothesis testing* to find the best fitting distribution. All the candidate models have one or more free parameters, so the hypothesis is the statement that the channel tap random variable is drawn from a distribution belonging to the Rayleigh, the Rice, the Nakagami etc. family. This is a different question than the one posed before, asking for the best approximating model from a family of a priori models. there are several problems associated with the hypothesis testing approach, especially that there is no universally adopted criterion to decide in favor of one out of many candidate models, since confidence levels, discretization and parameter estimation are always left unspecified. However, because the hypothesis testing approach is prevalent in fading channel modeling, we will focus on it. Some researchers propose to first estimate the parameters of all candidate PDFs and then perform the simple hypothesis test only for these parametrized PDFs. Yet though intuitively appealing, this method is not well justified for some tests.

6) *Hypothesis Testing*: The following is a short summary about hypothesis testing, extracted from the books by Papoulis [34], Bartoszyński [35] and Dixon [36]. Hypothesis testing is part of decision theory. The simplest case is the binary hypothesis testing problem, where some assumption, called the *null hypothesis*  $H_0$  is tested against the *alternate hypothesis*  $H_1$ . The null hypothesis might be for example the assumption that the distribution of a random variable  $X$  has parameter  $\theta = \theta_0$ . The alternate hypothesis would then be  $\theta \neq \theta_0$ . Hypothesis testing is not about determining whether  $H_0$  or  $H_1$  is true. It is to establish if the evidence in form of available data supports the hypothesis or not. Therefore the sample space is partitioned into the *critical region*  $\mathcal{D}_c$  and the *region of acceptance*  $\mathcal{D}_c^c$ . Depending on the location of the data points  $\mathbf{X}$  within the sample space, the hypothesis of the test is rejected or not. Some basic terminology in hypothesis testing is summarized as follows.

- If  $H_0$  is true and  $\mathbf{X} \in \mathcal{D}_c$ ,  $H_0$  is rejected, called a *Type I error*. The probability

$$\alpha = \mathbb{P}(\mathbf{X} \in \mathcal{D}_c | H_0) \quad (61)$$

is called the *significance level* of the test.

- If  $H_0$  is false and  $\mathbf{X} \notin \mathcal{D}_c$ ,  $H_0$  is accepted, called a *Type II error*. The probability of error is a function  $\beta(\theta)$ , called the *operating characteristic* (OC) of the test.
- The difference  $P(\theta) := 1 - \beta(\theta)$  is the probability of rejecting  $H_0$  when false, called the *power* of the test.

For so called “goodness-of-fit” tests,  $H_0$  does not involve parameters. The hypothesis is, that a given function  $F_0(x)$  equals the distribution  $F(x)$  of a random variable  $X$ ,  $H_0 : F(x) \equiv F_0(x)$  against  $H_1 : F(x) \neq F_0(x)$ . These types of tests normally rely on

some limiting behavior of a function of the data and the distribution under test, called the *test statistic*. The distribution of this test statistic converges to some other distribution if the data is indeed drawn according to the distribution under test. If not, then the test statistic will yield a value that would occur only with low probability according to the limiting distribution. This probability is set by the confidence level  $\alpha$  of the test, and hence hypothesis where the test statistic exceeds the value of the CDF  $Q(\alpha)$  need to be rejected.

a) *The Kolmogorov-Smirnov Test:* A common hypothesis test for distributions is the *Kolmogorov-Smirnov* test for continuous CDFs. It is based on the fact that the test statistic  $\sqrt{n}D_n := \sqrt{n} \sup_x |F_n(x) - F(x)|$  has a limiting CDF for  $n \rightarrow \infty$  which does not depend on the test CDF  $F$  and the empirical CDF  $F_n$ , derived from  $n$  samples of the process. Now, if a CDF with estimated parameters is used instead of the fixed CDF, this theorem no longer holds and the test result is meaningless [35].

Let  $F_i(x)$  be the empirical estimate of the CDF of the random variable  $X$  from the sample  $i$  and let  $F_n(x)$  be the empirical CDF obtained from  $n$  independent samples. Then the distance

$$D_n := \sup_x |F_n(x) - F(x)| \quad (62)$$

converges to zero a.s. for  $n \rightarrow \infty$ . Hence for large  $n$ ,  $D_n$  is close to zero if  $H_0$  is true and close to  $\sup_x |F_n(x) - F(x)|$  if  $H - 1$  is true. The distribution of  $\sqrt{n}D_n$  can be shown to converge to the Kolmogorov distribution

$$\lim_{n \rightarrow \infty} \mathbb{P}(\sqrt{n}D_n \leq z) = 1 - 2 \sum_{k=1}^{\infty} (-1)^{k-1} e^{-2k^2 z^2} =: Q(z). \quad (63)$$

The test should reject  $H_0$  if the observed value of the statistic  $\sqrt{n}D_n$  exceeds the critical value determined from the right tail of the distribution according to the significance level.  $Q(z)$  is tabulated in any standard textbook, eg. [35, Table A7]. The test has power 1 against any alternative in the limit  $n \rightarrow \infty$ .

The test only applies if the distribution  $F(x)$  of the null hypothesis is fixed. If the parameters need to be estimated from the samples, the corresponding distribution  $F^*(x)$  is now *random*, depending on the same samples as the ones used to determine the empirical distribution  $F_n$ , and the limiting distribution of  $\sqrt{n} \sup_x |F_n(x) - F^*(x)|$  is not given by  $Q(z)$ .

b) *The  $\chi^2$  Test:* The  $\chi^2$  test was originally developed to test a sample against a discrete distribution. The procedure can be extended to continuous distributions and it even works to some extent for distributions where the parameters need to be estimated. Some theory and explanations are summarized below. The general procedure is as follows:

- Partition the range of the random variable in intervals  $C_j$ . There is no rule how to choose these intervals, but a equidistant partition seems to make sense. Even for distributions with unlimited range, only a limited number  $r$  of intervals are needed, since only intervals containing measured data points are necessary.
- Count the number  $N_j$  of measurements that lie in each interval  $j$ .
- Either estimate the parameters  $\Theta$  of the distribution under test from the unpartitioned or the partitioned data. See Appendix IV-C.6 for elaboration.
- Compute the test statistic according to (67) or (70), depending on the type of parameter estimate.
- compare the statistic to the integral over the right tail of the  $\chi_{r-1-k}^2$  PDF at confidence level  $\alpha$  and with  $r - 1 - k$  degrees of freedom, or equivalently the value of the CDF  $Q(1 - \alpha)$ . Here  $k$  is the number of parameters estimated from the data. Hence the number of degrees of freedom of the distribution is reduced if parameters need to be estimated first. If the test statistic is larger than the probability obtained by evaluating the integral, the hypotheses must be rejected.

### Discrete Distribution

Let  $X$  be a discrete random variable defined on some finite alphabet  $\mathcal{X}$  with associated probabilities  $p_i = \mathbb{P}(X = x_i)$ . In a random sample of size  $N$ , each letter appears with frequency  $N_i$ , such that  $\sum N_i = N$ . The vector  $[N_1, \dots, N_r]$  is called the *count vector*. The hypothesis to test is

$$H_0 : p_i = p_i^0, \quad i = 1, \dots, r \quad (64)$$

against the general alternative  $H_1: H_0$  is false. Here  $\mathbf{p}^0 = [p_1^0, \dots, p_r^0]$  is some fixed distribution. The test statistic

$$Q^2 := \sum_{j=1}^r \frac{(N_j - np_j^0)^2}{np_j^0} \quad (65)$$

has the limiting distribution  $\chi_{r-1}^2$ , i.e. a central  $\chi^2$  distribution with  $r - 1$  degrees of freedom, if the distribution of  $X$  equals the distribution of the null hypothesis. To obtain a good approximation, the counts should exceed 10. When there are many letters in the alphabet, the approximation is good enough even if few expected frequencies are as small as 1. The critical region of the test is the right tail of the  $\chi^2$  distribution with confidence level  $\alpha$ , denoted  $\chi_{\alpha, r-1}^2$  and tabulated in any standard statistics textbook [35, Table A4]. If now the test statistic exceeds this value, then the distribution of the sample can be only be drawn according to the distribution under test with low probability (with probability less than  $\alpha$  to be precise). Hence this hypothesis has to be rejected.

### Continuous Distribution

The above outlined test can be adapted to continuous distributions by partitioning the range of the random variable  $X$ , i.e. by creating  $r$  sets  $C_1, \dots, C_r$  that are disjoint and cover the whole range<sup>10</sup>. If  $f(x)$  is the density of  $X$  specified by the null hypothesis, then

$$p_j^0 = \int_{C_j} f(x) dx, \quad j = 1, \dots, r. \quad (66)$$

The test now depends also on the choice of partition.

### Discrete Parametric Distribution

Often the Distribution of the null hypothesis is not completely specified, such that just the family (e.g. Bernoulli, Poisson etc.) is known and the parameters are not. Denote the  $k$ -dimensional parameter vector by  $\Theta$ . Then the distribution of the discrete random variable  $X$  is given by  $\mathbf{p}(\Theta) = [p_1(\Theta), \dots, p_r(\Theta)]$  with  $p_j(\Theta) > 0$ . Let the maximum likelihood estimate (MLE) of  $\Theta$  be denoted by  $\hat{\Theta}$ . Then the statistic

$$Q^2 := \sum_{j=1}^r \frac{[N_j - np_j(\hat{\Theta})]^2}{np_j(\hat{\Theta})} \quad (67)$$

has the limiting  $\chi^2$  distribution with  $r - 1 - k$  degrees of freedom as  $n \rightarrow \infty$ . Thus the test proceeds as before, but to compute the critical region, the distribution with the reduced number of degrees of freedom needs to be used.

### Continuous Parametric Distribution

If the parametric distribution is continuous, the test methodology remains the same, i.e. the range of  $X$  needs to be partitioned and the respective probabilities are computed via the integral over the density function. However, the MLE of the parameter vector is now in general very hard to obtain. The key point is that  $\Theta$  is no longer the the same for the continuous distribution and the discrete distribution obtained through partitioning. However, it is the latter MLE that is required to form the statistic (67). In most cases,  $\hat{\Theta}$  can only be obtained numerically. An example borrowed from Bartoszyński [35] illustrates this problem. Assume  $X \sim \mathcal{N}(\mu, \sigma^2)$  and  $N_j$  is the count of observations in the interval  $[t_{j-1}, t_j]$ . The MLE is the solution to the system of equations

$$\frac{\partial \log L}{\partial \mu} = 0, \quad \frac{\partial \log L}{\partial (\sigma^2)} = 0 \quad (68)$$

with the likelihood function

$$L = \prod_{j=1}^r \left( \frac{1}{\sqrt{2\pi\sigma^2}} \int_{t_{j-1}}^{t_j} e^{-\frac{(x-\mu)^2}{2\sigma^2}} dx \right)^{N_j}. \quad (69)$$

If now the MLE from the complete data instead of the grouped data is used, the limiting distribution is unknown. However, there exists a bound. Let  $\hat{\Theta}^*$  be the MLE of the parameter vector based on the complete observation. Then the statistic

$$Q^{*2} := \sum_{j=1}^r \frac{[N_j - np_j(\hat{\Theta}^*)]^2}{np_j(\hat{\Theta}^*)} \quad (70)$$

satisfies, as  $n \rightarrow \infty$

$$\Pr(\chi_{r-1-k}^2 \geq t) \geq \lim_{n \rightarrow \infty} \Pr(Q^{*2} \geq t) \geq \Pr(\chi_{r-1}^2 \geq t) \quad (71)$$

for every  $t \geq 0$ . This implies that if the hypothesis can be rejected on the basis of the partitioned distribution with the unpartitioned parameter estimates, it will also be rejected if the partitioned parameter estimates are used.

### 7) Parameter Estimation:

*a) Nakagami  $m$  Parameter:* Maximum likelihood estimation of the Nakagami parameters  $\Omega$  and  $m$  is not possible in closed form. Several approximations to the true ML solution exist, like the estimators recently proposed by Cheng [37] and Ko [38], and the classical approximation by Greenwood and Durand [39], recently reintroduced by Zhang [40]. The latter ML approximation is in effect for the gamma distribution, but since the square of a Nakagami distributed random variable is gamma distributed, the estimates are equivalent. It is difficult to compare the performance of the various estimators

*b) Delay Spread:* Mean delay and delay spread are tied to the uncorrelated scattering assumption. In this case, the correlation matrix of the channel is diagonal, and can be obtained by averaging several measured impulse responses, also referred to as the power delay profile. The mean delay is now the mean of the PDP, the delay spread the standard deviation. Thus both parameters together are a measure about the number of independently fading taps and thus about the diversity order, although not in a precise way as analyzed above. For these numbers to be meaningful, the PDP needs to be compactly supported and also otherwise mathematically well behaved, an assumption which can almost always be made for the channels under consideration.

<sup>10</sup>The sets need not necessarily be intervals.

In the following, we estimate the mean delay  $\bar{\tau}$  and the delay spread  $s$  of every recorded impulse response in the different environments and for different separations between receiver and transmitter. All impulse responses are normalized to have unit energy. Then the mean delay is given as  $\bar{\tau} = \sum_{l=1}^L \tilde{h}[l]l$  and the delay spread as  $s = \sqrt{\sum_{l=1}^L (l - \bar{\tau})^2 \tilde{h}[l]}$  where  $\tilde{h}$  is the normalized channel impulse response. The average empirical mean delay is recorded as  $\mu\bar{\tau}$ , the standard deviation as  $\sigma_{\bar{\tau}}$ ; the same quantities are also computed for the empirical delay spread  $s$ .

## APPENDIX V IMPULSE RESPONSES FOR SIMULATIONS

The selection criteria document for IEEE 802.15.4a demands that simulations are done with 100 predefined impulse responses for each environment, each of which is normalized to unit energy. The following section gives the references to the Excel files that contain the impulse responses, as well as critical parameters from those impulse responses. The format for all XLS files referenced in this section is:

### A. Body area network

The files are "front.xls", "side.xls", and "back.xls". The parameters obtained with that model are

FRONT: delay spread = 0.2 ns. Mean number of MPCs within 15 dB = 3.5

SIDE: delay spread = 1.2 ns. Mean number of MPCs within 15 dB = 5.2

BACK: delay spread = 3.3 ns. Mean number of MPCs within 15 dB = 7.9

### B. Open Farm Environment

Model Characteristics

Mean delays: excess (tau\_m) = 28.1 ns, RMS (tau\_rms) = 17

# paths: NP\_10dB = 4.2, NP\_85% = 5.0

## Bibliography

In the following, those references are cited that have a single- or double-digit reference number. References with the format [0y-xxx] and [04-xxx] refer to IEEE standards documents; the full official Document control Number of those documents reads P802.15-0y-xxx-r-004a, where y denotes the year, xxx the document number, and r the revision number of the document.

## REFERENCES

- [1] G. Kadel and R. Lorenz, "Impact of the radio channel on the performance of digital mobile communication systems," in *Sixth IEEE Int. Symp. on Personal, Indoor and Mobile Radio Communications PIMRC'95*, pp. 419–423, 1995.
- [2] J.-P. Rossi, "Influence of measurement conditions on the evaluation of some radio channel parameters," *IEEE Trans. on Vehicular Technology*, vol. VT-48, pp. 1304–1316, July 1999.
- [3] R. Qiu and I.-T. Lu, "Wideband wireless multipath channel modeling with path frequency dependence," in *IEEE International Conference on Communications (ICC'96)*, 1996.
- [4] R. C. Qiu and I. Lu, "Multipath resolving with frequency dependence for broadband wireless channel modeling," *IEEE Trans. Veh. Tech.*, 1999.
- [5] U.C.A.N., "Report on UWB basic transmission loss," Tech. Rep. IST-2001-32710, IST-2001-32710, Mar. 2003.
- [6] S. S. Ghassemzadeh, R. Jana, C. W. Rice, W. Turin, and V. Tarokh, "A statistical path loss model for in-home UWB channels," in *IEEE Conference on Ultra Wideband Systems and Technologies Digest of Technical Papers*, pp. 59–64, 2002.
- [7] S. S. Ghassemzadeh and V. Tarokh, "The ultra-wideband indoor path loss model," Tech. Rep. P802.15 02/277r1SG3a, AT&T Labs, Florham Park, NJ, USA, June 2002. IEEE P802.15 SG3a contribution.
- [8] S. Ghassemzadeh, L. Greenstein, T. Sveinsson, A. Kavcic, and V. Tarokh, "Uwb indoor path loss model for residential and commercial environments," in *IEEE VTC 2003- Fall*, 2003.
- [9] S. Ghassemzadeh, R. Jana, C. Rice, W. Turin, and V. Tarokh, "Measurement and modeling of an ultra-wide bandwidth indoor channel," *IEEE Transaction on Commun.*, pp. 1786–1796, 2004.
- [10] J. O. Nielsen, G. F. Pedersen, K. O. K., and I. Z. K. I.Z., "Statistics of measured body loss for mobile phones,"
- [11] A. Saleh and R. A. Valenzuela, "A statistical model for indoor multipath propagation," *IEEE J. Selected Areas Comm.*, vol. 5, pp. 138–137, Feb. 1987.
- [12] M. Steinbauer and A. F. Molisch, *Directional Channel Modelling*. Wiley, 2001.
- [13] J. Karedal, S. Wyne, P. Almers, F. Tufvesson, and A. F. Molisch, "Statistical analysis of the uwb channel in an industrial environment," in *Proc. VTC fall 2004*, 2004.
- [14] T. S. Rappaport 1989.
- [15] W. Pietsch 1994.
- [16] D. Cassioli, M. Z. Win, and A. F. Molisch, "The ultra-wide bandwidth indoor channel: From statistical models to simulations," vol. 20, pp. 1247–1257, Aug. 2002.
- [17] K. Siwiak, H. Bertoni, and S. M. Yano, "Relation between multipath and wave propagation attenuation," *Electronics Letters*, vol. 39, pp. 142–143, Jan. 2003.
- [18] D. Cassioli, M. Z. Win, and A. F. Molisch, "A statistical model for the UWB indoor channel," in *Proc. 53<sup>rd</sup> IEEE Vehicular Technology Conference*, vol. 2, pp. 1159–1163, May 2001.
- [19] P. A. Bello, "Characterization of randomly time-variant linear channels," vol. 11, pp. 360–393, 1963.
- [20] H. Artés, G. Matz, and F. Hlawatsch, "Linear time-varying channels," Tech. Rep. 98-06, Department of Communications and Radio-Frequency Engineering, Vienna University of Technology, Vienna, Austria, Dec. 1998.
- [21] J. Kunisch and J. Pamp, "Measurement results and modeling aspects for the UWB radio channel," in *IEEE Conference on Ultra Wideband Systems and Technologies Digest of Technical Papers*, pp. 19–23, 2002.
- [22] G. Matz, "characterization of non-WSSUS fading dispersive channels," in *Proc. Int. Conference on Communications*, pp. 2480–2484, May 2003.

- [23] H. Hashemi, "The indoor radio propagation channel," vol. 81, pp. 943–968, July 1993.
- [24] R. C. Qiu, "A study of the ultra-wideband wireless propagation channel and optimum UWB receiver design," vol. 20, pp. 1628–1637, Dec. 2002.
- [25] M. Hämäläinen, T. Pätsi, and V. Hovinen, "Ultra wideband indoor radio channel measurements," in *Proc. 2<sup>nd</sup> Finish Wireless Communications Workshop*, (Tampere, Finland), Oct. 2001.
- [26] A. S. Y. Poon and M. Ho, "Indoor multiple-antenna channel characterization from 2 to 8 GHz," in *Proc. Int. Conference on Communications*, May 2003.
- [27] Á. Álvarez, G. Valera, M. Lobeira, R. Torres, and J. L. Garcia, "Ultrawideband channel characterization and modeling," in *Proc. Int. Workshop on Ultra Wideband Systems*, (Oulu, Finland), June 2003.
- [28] J. Keignart and N. Daniele, "Channel sounding and modelling for indoor UWB communications," in *Proc. Int. Workshop on Ultra Wideband Systems*, (Oulu, Finland), June 2003.
- [29] P. Pagani, P. Pajusco, and S. Voinot, "A study of the ultra-wide band indoor channel: Propagation experiment and measurement results," in *Proc. Int. Workshop on Ultra Wideband Systems*, (Oulu, Finland), June 2003.
- [30] A. F. Molisch, J. R. Foerster, and M. Pendergrass, "Channel models for ultrawideband personal area networks," *IEEE Personal Communications Magazine*, vol. 10, pp. 14–21, Dec. 2003.
- [31] Q. H. Spencer, B. D. Jeffs, M. A. Jensen, and A. L. Swindlehurst, "Modeling the statistical time and angle of arrival characteristics of an indoor multipath channel," vol. 18, pp. 347–360, Mar. 2000.
- [32] V. Erceg, L. Schumacher, P. Kyritsi, D. S. Baum, A. F. Molisch, and A. Y. Gorokhov, "Indoor MIMO WLAN channel models," in *Standardization drafts of IEEE 802 meeting Dallas, March 2003*, 2003.
- [33] H. Akaike, "Information theory and an extension of the maximum likelihood principle," in *Breakthroughs in Statistics* (S. Kotz and N. L. Johnson, eds.), vol. 1, pp. 610–624, New York, NY, USA: Springer, 1992. originally published in the Proceedings of the second International Symposium on Information Theory, Budapest, 1973.
- [34] A. Papoulis and S. U. Pillai, *Probability, Random Variables and Stochastic Processes*. Boston, MA, USA: McGraw-Hill, fourth ed., 2002.
- [35] R. Bartoszyński and M. Niewiadomska-Bugaj, *Probability and Statistical Inference*. New York, NY, USA: Wiley, 1996.
- [36] W. J. Dixon and F. J. Massey, Jr., *Introduction to Statistical Analysis*. New York, NY, USA: McGraw-Hill, fourth ed., 1983.
- [37] J. Cheng and N. C. Beaulieu, "Maximum-likelihood based estimation of the Nakagami  $m$  parameter," vol. 5, pp. 101–103, Mar. 2001.
- [38] Y.-C. Ko and M.-S. Alouini, "Estimation of Nakagami- $m$  fading channel parameters with applications to optimized transmitter diversity systems," 2003.
- [39] J. A. Greenwood and D. Durand, "Aids for fitting the gamma distribution by maximum likelihood," *Technometrics*, vol. 2, pp. 55–66, Feb. 1960.
- [40] Q. T. Zhang, "A note on the estimation of Nakagami- $m$  fading parameter," 2002.